Ionics (2020) 26:1563–1589
https://doi.org/10.1007/s11581-020-03473-0

REVIEW

Heteroatom- and metalloid-doped carbon catalysts for oxygen reduction reaction: a mini-review

Shaik Gouse Peera[1] · Hyuk-Jun Kwon[1] · Tae Gwan Lee[1] · A. Mohammed Hussain[2]

Received: 18 October 2019 / Revised: 20 December 2019 / Accepted: 24 January 2020 / Published online: 6 February 2020

Abstract

Electrocatalysts for oxygen reduction reaction have been the study of interest because of their importance in various energy storage and conversion reactions. Though platinum-based catalysts are found to be the most active catalysts for oxygen reduction reactions, their high cost and scarcity have led researchers to discover alternative active and cost-effective catalysts. In this regard, heteroatom- and metalloid-doped catalysts were explored as possible alternatives to traditional platinum-based catalysts. Consequently, a large number of heteroatom- and metalloid-doped catalysts have been synthesized and evaluated for oxygen reduction activity. Synergistic catalysts, with dual-doped, tri-doped, and multi-heteroatom-doped catalysts, were also synthesized by doping more than one heteroatom. In this review, we discuss the fundamental principles and reasons behind the origin of ORR catalysis of heteroatom- and metalloid-doped catalysts discussed with the support of literatures.

Keywords Fuel cells · Oxygen reduction reaction · Heteroatom doping · Metalloid catalysts · Metal-free catalysts

Introduction

Increasing energy crisis due to an ever-growing population demands the requirement of advanced energy generation technologies, especially for transport applications. State-of-the-art emerging technologies include rechargeable batteries, high-energy-density supercapacitors, and high-power-density fuel cells [1–3]. Among these, fuel cell technologies are promising in view of high-power density and nearly zero emission and most importantly it allows a continuous operation, if reactants are constantly supplied. There are various types of fuel cells, among them proton exchange membrane fuel cells (PEMFCs) and anion exchange membrane fuel cells (AEMFCs) which are of particular interest for transportation applications. In both types of fuel cells, hydrogen (H_2) acts as a fuel and O_2/air acts as an oxidant. The H_2 gas is oxidized at the anode and O_2 reduces at the cathode, producing H_2O as the final product at the cathode. The electrons generated at the anode, after H_2 oxidation, perform the electrical work and are utilized at the cathode to reduce O_2 to H_2O. The slower kinetics of oxygen reduction reaction (ORR) that occur at the cathode actually determines the overall power density of the fuel cells. The state-of-the-art catalyst used for ORR is platinum (Pt) or Pt-alloy nanoparticles supported on a high surface area carbon [4–6]. The ORR activity of Pt nanoparticles is high, compared with any other metallic nanoparticles in the periodic table; Pt/C has become the only choice of catalysts for fuel cells so far for practical applications. However, the use of the Pt/C catalyst tremendously increases the cost of fuel cells, and hence developing alternative, cheap, and earth-abundant catalysts is highly desirable, in order to make the fuel cell technologies in an affordable price. Development of cost-effective catalysts without compromising the high ORR activity and durability needs a basic understanding on the identification of ORR active sites, reaction kinetics, interactions of active sites with gaseous O_2, energy barriers for O_2 adsorption, electron transfer between the substrate and gaseous reactants of ORR reactions, etc. Understanding the effect of each of these parameters is so important, in order to manipulate the electronic configurations and geometries around the ORR active sites, to effectively lower the energy requirements for efficient O_2 reduction. This article overviews the fundamental aspects and

✉ Shaik Gouse Peera
gouse@kmu.ac.kr; gousechem@gmail.com

✉ Tae Gwan Lee
wateree@naver.com

[1] Department of Environmental Science and Engineering, Keimyung University, Daegu 42601, Republic of South Korea

[2] Energy Research Center, University of Maryland, College Park, MD 20740, USA

motivations behind the development of such alternative and cheap catalysts with heteroatom- and metalloid-doped catalysts developed in recent literatures. The first section of this article deals with heteroatom-doped catalysts, followed by a second section in which metalloid catalysts are discussed.

Heteroatom-doped (metal-free) catalysts

Since a few decades, researchers have come up with wide varieties of alternative catalysts which include earth-abundant catalysts such as transition metal–based catalysts [7, 8]. The most popular transition metals utilized for ORR are Fe- and Co-based catalysts [9–11]. As such, the metallic nanoparticles of Fe and Co exhibit reasonable ORR activity. However, the activity of these metallic nanoparticles enhances several folds when they are incorporated together with heteroatoms such as N, P, S, B, and halogens, especially with N doping. When they are incorporated with N-doped carbon, a special bonding configuration called metal coordination to nitrogen species of carbon (M–N–C) are formed, and many researchers are convinced that the activity of transition metal–derived catalysts comes from these M–N–C active sites [12, 13].

On the other hand, the doping of heteroatoms themselves is found to induce the carbon matrix into a catalytically active site, without the help of any metal species, so-called metal-free catalysts [14]. Heteroatom-doped carbon materials have evolved as metal-free ORR catalysts, which is considered as a revolutionary breakthrough in the field of catalysis, which includes both energy storage and conversion technologies [15]. They have been paid much attention in the past two decades as they can be easily synthesized and they are inexpensive compared with metal-based catalysts. Moreover, they show high catalytic activity and stability in both acidic and alkaline electrolytes. Due to this, enormous research is dedicated to develop heteroatom-doped catalysts and understand their kinetic behavior. Heteroatom-doped carbon materials such as carbon nanotubes, carbon nanofibers, graphitic mesoporous carbons, and graphene are extensively investigated as metal-free catalysts. As a general aspect, all sp2 carbon materials contain a σ bond formed by the hybridization of s, p_x, and p_y atomic orbitals and a π bond formed with the p_z orbital (valence band) with an empty π* orbital (conduction band) (Fig. 1). Hence, sp2 carbon–containing materials can be considered as metal or zero band gap semiconductors. However, the absence of an intrinsic band gap restricts their wide-range applications [16–18].

Chemical doping of foreign heteroatoms, in which carbon atoms are replaced by the heteroatoms, is considered as an effective way in band gap engineering, modifying the electronic and surface properties of carbon nanomaterials [19, 20]. "Various foreign heteroatoms such as nitrogen (N), sulphur (S), boron (B), phosphorus (P) and halogens such as fluorine (F), chlorine (Cl), bromine (Br), iodine (I) and are proposed in the literatures as effective chemical dopants to the carbon nanomaterials" [21–27]. Due to the electronegativity difference between carbon and heteroatoms, an induced polarization network, i.e., positive/negative charges on the adjacent carbon, occurs, thereby facilitating ORR. This polarization network also influences the magnetic, optical, and electronic properties of the doped carbons [28]. By the doping of heteroatoms, neighboring C atoms experience different charge and spin densities, which also provide surface active sites facilitating the effective electron transfer [29].

Different heteroatoms catalyze electrochemical O_2 reduction differently, based on their binding configurations in carbon support, electronegativity of the heteroatom with that of carbon, number of valence electron, and influence on charge and spin density on neighboring C atoms. For instance, N doping effectively opens the band gap between the conduction band and the valence band by shifting the Dirac point above the Fermi level. N doping changes the charge and spin densities of adjacent C atoms, which attracts the gaseous O_2 for its subsequent reduction to H_2O, due to the higher electronegativity of N compared with C. This electronegativity difference brings out the different electron density distribution of neighboring C atoms around the N-doped sites [30]. Generally, there are four types of N configurations, namely, pyridinic N, pyrrolic N, quaternary N/graphitic-N, and N-oxides of pyridinic N. All these configurations can be identified with the help of their different binding energies by X-ray photoelectron spectroscopy (XPS) analysis. In terms of their bonding configurations, the pyridinic type of N species usually exists at the defect or edge sites of the carbons, and introduces its one-π electron pair to the aromatic π system. Pyrrolic N is a five-membered heterocyclic configuration, which bonds with two carbon atoms and contributes two π electrons to the aromatic π system. Quaternary-N/graphitic-N atoms present in the plane of carbon sheets by replacing the C atoms in the plane within the hexagonal ring. There is also the configuration in pyrrolic-N atoms bonded to two carbon atoms and one oxygen atom pyridinic-N^+-O^-. Still, there is a debate in the literature as to which of these bonding configurations are most active in the ORR process. Many theoretical calculations were performed through density functional theory (DFT) and by experimental evaluation; it is convinced that graphitic-N and pyridinic-N are found to be ORR active.

Sulfur (S) doping induces a higher spin density rather than charge density, since S has an electronegativity (2.58) close to that of carbon (2.55). Similar to N atoms, S atoms are incorporated into the sp2 carbon lattice. Due to the similar electronegativity values, S doping has a low effect on electronic charge distribution. Hence, the origin of high ORR activity of S-doped carbons is due to the spin density, rather than charge density [31]. Boron (B) doping induces p-type electrical properties to carbon materials. The enhanced charge

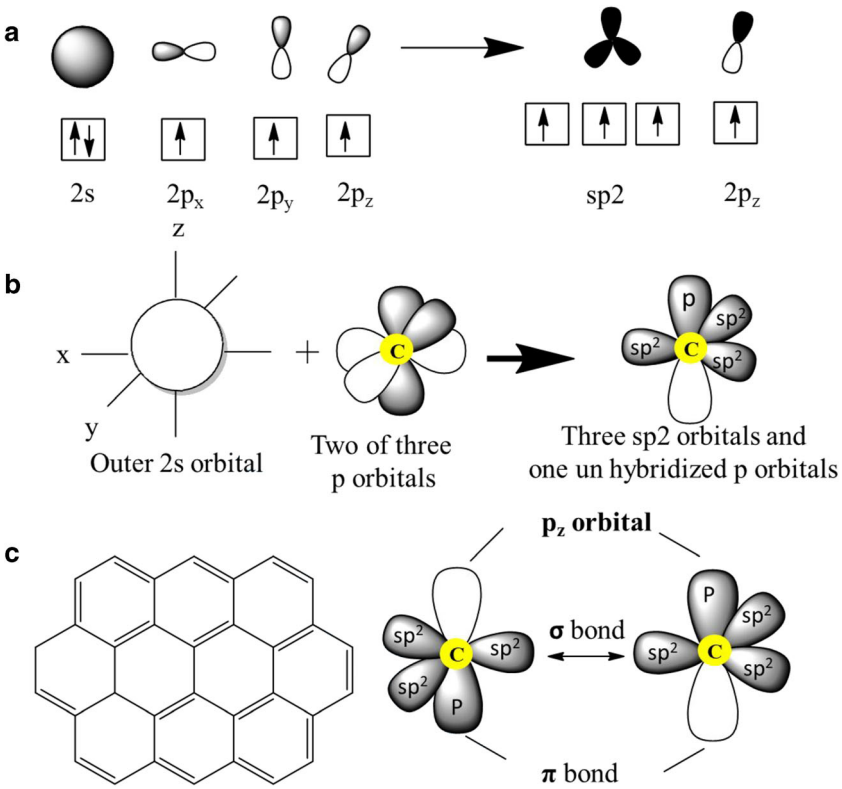

Fig. 1 **a** Atomic C-hybridization. **b** C hybridization in carbon-based materials. **c** Hybridized carbon atoms by covalent bonds [σ and π bonds induce a double covalent bond between two carbon atoms, p_z orbital possesses a free delocalized electron permitting the electronic conductivity]

polarization and carrier concentration greatly enhance the electrical properties of the B-doped carbons, favoring O_2 reduction kinetics [32]. Another heteroatom from the nitrogen group elements is phosphorus (P), with a lower electronegativity (2.19) and a larger covalent radius than that of N. Hence, the C–P bond polarity is exactly opposite to that in N–C configurations. Moreover, P atoms protrude out of the hexagonal carbon network due to the different bond length of P–C (1.79 Å), whereas it is 1.42 Å for C–C. This difference in bond length induces a strain and forces P to protrude from the basal hexagonal carbon network, facilitating the O_2 reduction kinetics. Formation of C–P–O bonds is found to be more effective and stable for ORR [33]. In addition, P doing is found to be more effective in anti-poisoning effects towards various molecules such as SO_x, NO_x, and PO_x ions, which is beneficial for ORR catalysts [34]. Halogen (F, Cl, Br, and I)-doped carbon materials are also proposed to have admirable ORR activity. However, in some reports the concept of electronegativity did not give the best concluding remarks as the ORR activity of the halogens did not follow based on electronegativity. In this case, the atomic size of the halogens seems to play an important role in inducing enhancement of the charge transfer during ORR. Other reports still explain the halogen-doped carbon catalysts in terms of electronegativity. Hence, the exact nature of the halogen-doped carbons is yet to be analyzed perfectly and still remains an unsolved problem.

In general, doping of heteroatoms is performed in three different ways. Firstly, the pre-synthesized carbons are doped with precursors which contain heteroatoms such as melamine, urea, thiourea, g-C_3N_4, and NH_3 gas [35–37]. Secondly, the heteroatom-containing precursors are pyrolyzed directly, to yield heteroatom-doped carbons such as polyaniline, polypyrrole, sulfonated polyaniline, and gelatin [38–41]. Thirdly, the biomass materials are pyrolyzed to synthesize the heteroatom-doped catalysts [42–45]. Often, temperature optimization is required to ensure the complete removal of the precursors, which affect the catalytic properties; pyrolysis temperature has great influence on the type of dopant species and their relative abundance in the final catalyst.

Mono-doped carbons as ORR catalysts

As stated earlier, N doping creates active sites by changing the local spin and charge density of the carbons, imparting a catalytic activity towards ORR. However, there are lots of controversies on ORR active sites of N-doped carbons such as which type of N is solely responsible for the ORR activity as well as the influence of carbon structure on the doping of N, which is still a debatable topic [46]. Moreover, N-doped carbon activity is highly dependent on the position of doping. It is well known that edge-doped heteroatoms are far more active than basal plane heteroatoms [47, 48]. A significant amount of research was carried out on heteroatom-doped catalysts for ORR, especially starting from N doping to the carbons, when Gong et al., [49] described the effect on N doping on the vertically aligned nitrogen-doped carbon nanotubes (VA-

NCNTs). The N-doped VA-NCNTs catalyze effective 4-electron ORR with excellent anti-CO poisoning effects. Their density functional theory calculations suggest that N doping to VA-CNTs significantly changes the O_2 adsorption mode from end-on (Pauling model) to side-on (Yeager model). The effective change transfer from N atoms to the adjacent C atoms and side-on adsorption effectively weakens the O–O bond and hence reduces the overall potential of ORR. This particular study has motivated researchers to conduct a deeper investigation on the N-doped carbons towards ORR. Followed by this report, Dai et al. [50] synthesized N-doped graphene by a chemical vapor deposition with ammonia as a nitrogen source. The synthesized N-graphene shows extraordinary ORR activity over undoped graphene with an admirable stability and a dominant 4-electron transfer process and complete resistance to the methanol and CO poising effects in alkaline electrolytes. Followed by this large number of N-doped carbons are the proposed metal-free ORR catalysts [51–54]. Oh et al. [55] synthesized N-doped carbon black as an excellent electrocatalyst for oxygen reduction reaction with melamine as a nitrogen source. The resulting N-CB-750-1000 catalyst showed excellent ORR activity, surpassing Pt/C. Research reports also suggest that pyrolysis temperature has great influence on the type of N species and their relative abundance. For instance, Deng et al. [56] synthesized N-CNTs by the controlled polymerization of polyaniline followed by the pyrolysis process. It is found that there is a direct relationship between the pyrolysis temperature and the abundance of different N species. The polyaniline-polymerized CNTs are pyrolyzed at different temperatures from 700 to 900 °C. The XPS analysis of NCTNs shows that there is a drastic decrease in the N content from 6.72 to 1.78% when the pyrolysis temperatures are between 700 and 900 °C. The decrease in pyrrolic-N is observed when the pyrolysis temperatures are higher, due to the low thermal stability of pyrrolic-N [57]. Contrastingly, the abundance of pyridinic-N and graphitic-N is observed. This is due to their higher thermal stability, when compared with pyrrolic-N [58]. Among all the catalysts, the NCT-700 catalyst shows a higher ORR activity, with an ORR onset potential of 0.84 V. The enhanced ORR activity is due to the higher percentage of graphitic-N and pyridinic-N [59–61]. The electron backdonation from graphitic-N to the carbon matrix, and in turn to the oxygen antibonding orbitals, makes graphitic-N active towards ORR (Fig. 2a, b). Pyridinic-N has a lone pair of electrons which are not donated to the carbon matrix and are freely accessible to O_2, and hence, pyridinic-N would principally be more active than the other forms of N [59–61]. A large number of reports made on N doping to the various types of carbons such as carbon nanosheets, graphene, carbon nanotubes, and graphene quantum dots have been proposed [51, 62–69].

Recently, metal organic framework (MOF)–derived metal-free catalysts have emerged as a new class of advanced materials in various fields of catalysis [70–72]. Depending on metal coordination and ligand type, MOFs with various topology and geometries can be derived. As the MOF contains a ligand with heteroatoms such as N and S and metal atoms together, pyrolysis of the MOF structures generates heteroatom-doped metal catalysts simultaneously. Most MOF-derived catalysts reported are with Zn as the metal atom and 2-methylimidazole as a ligand and the most popular methods of MOF synthesis include solvothermal, hydrothermal, sonochemical, microwave, and electrochemical methods [73–77]. In all the MOF-derived catalysts, the precursors are subjected to the pyrolysis process at a boiling point temperature of Zn (908 °C), where the Zn atoms are converted into ZnO and subsequently to metallic Zn. Metallic Zn is carried away from the catalyst by a carrier inert gas, yielding a catalyst with no Zn atoms. The main advantage of MOF-derived catalysts is evaporation of metallic Zn and release of CO_2 gases which imparts an intrinsic porous nature to the catalysts [78]. For example, Zhang et al. [79] synthesized a polyhedral-shaped graphitized N-doped carbon from Zn-based ZIF-8 precursors. NGPCs show unique porous structures, with a high BET surface area of 932 $m^3\ g^{-1}$ and high graphitization, with a high pyridinic-N content. Moreover, the NGPC-1000-10 catalyst also showed excellent ORR activity close to the commercial Pt/C catalyst in the alkaline electrolyte, with nearly a four-electron reduction reaction. Wu reported polyhedral ZIF-8 crystals and pyrolyzed at 900 °C to obtain porous N-doped carbons (NPC-900). The NPC-900 catalyst is further activated with NH_3. It is observed that after NH_3 activation, a higher graphitic-N content is observed due to etching of the carbon surface (NHPC-900). The NHPC-900 catalyst shows excellent ORR activity over the Pt/C catalyst [80]. Followed by this, a large number of studies have been performed to synthesize the porous N-doped carbons, and the summary of these can be found in [81–87].

With an electron withdrawing ability, B could also be a good choice as dopant to carbon-based materials. Sheng et al. [88] synthesized boron-doped graphene (BG) by a thermal annealing of graphite oxide with boric acid. Thermal removal of oxygen functionalities in the graphene oxide frameworks provides active sites for the successful doping of B atoms in the carbon frameworks. The ORR analysis of BG shows a noticeable ORR onset potential in the 0.1-M KOH electrolyte, but which is much inferior to the Pt/C catalyst. However, the number of electrons calculated from the K–L plots is found to be 3.5 e^-, suggesting the possibility of H_2O_2 formation during the ORR process. In another study, Bo et al. [89] synthesized B-doped mesoporous carbon BOMCs-2, as an ORR catalyst, whose activity is still inferior to Pt/C in the alkaline medium. In another, Yang et al. [90] synthesized boron-doped carbon nanotubes, and again the ORR activity of BCNTs is still inferior to the Pt/C catalyst. DFT studies performed in this study suggest that B–C_3 and B–C bonds

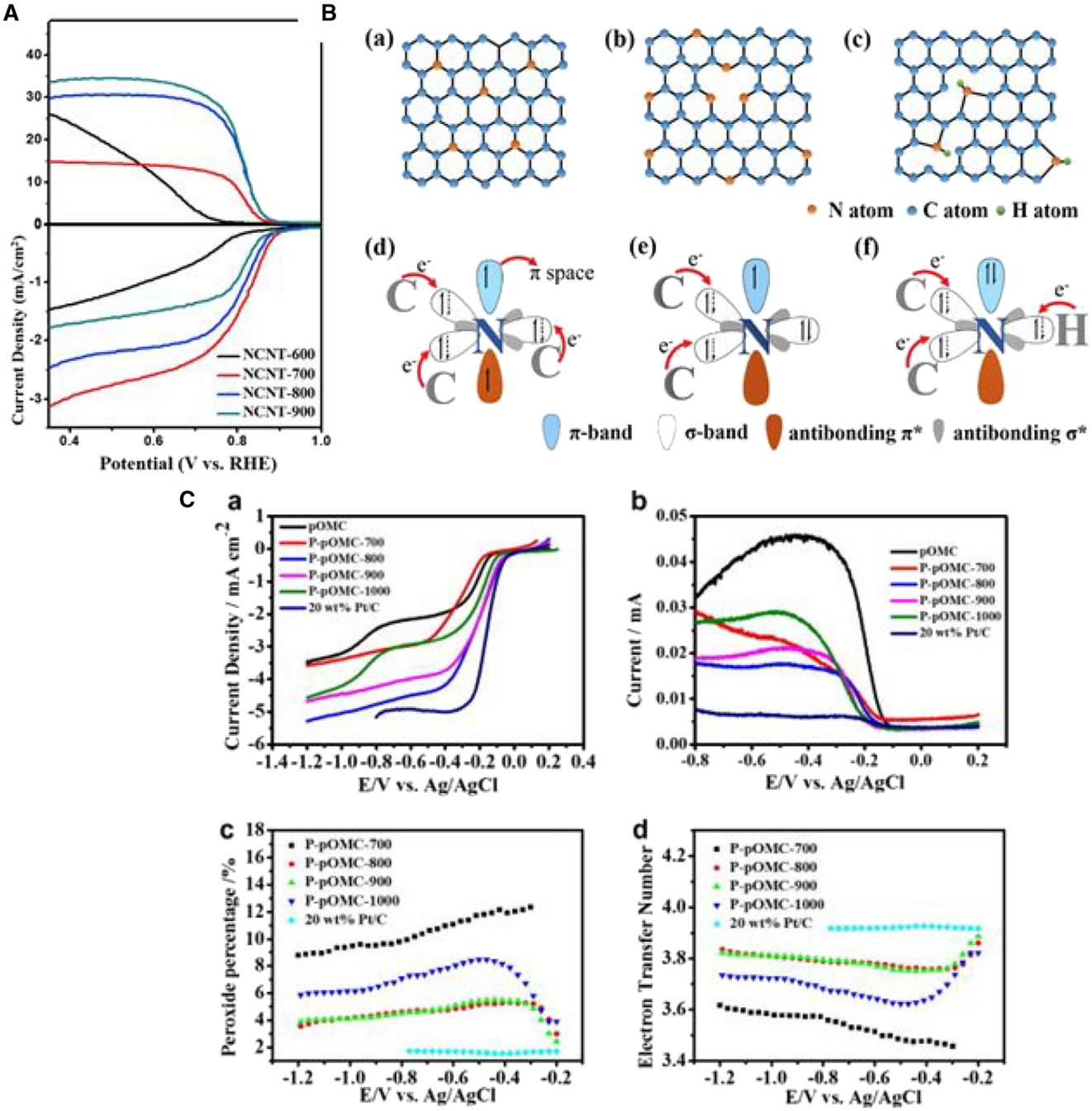

Fig. 2 **a** LSV curves of ORR over NCNT materials on RRDE at a fixed rotation rate of 1600 rpm in an O_2-saturated 1-M NaOH electrolyte at a scan rate of 5 mV s^{-1}. **b** Three types of N–C bonding configurations existed in the NCNTs: graphite N, pyridine N, and pyrrolic N. A schematic representation of the doped atom electronic structure [56] Reprinted with permission from ref. 56 Copyright 2017 Elsevier. **c** Steady-state RRDE experiments of P-pOMC, pOMC, and 20 wt.% Pt/C (E-TEK) catalysts for ORR at the 1600-rpm electrode rotation rate and 10 mV s^{-1} potential scan rate. Disk (a) and ring (b) current are shown separately for convenient viewing, (c) plot of percentage of peroxide formation, and (d) number of electron transfer at different potentials for P-pOMC and 20 wt.% Pt/C (E-TEK) catalysts for ORR [93] Reprinted with permission from ref. 93 Copyright 2014 Elsevier

are polarized due to the high electronegativity of carbon, creating polarized bonds in the CNTs, which subsequently interact with O_2. Therefore, doping a low-electronegativity B can transform its electron-deficient nature into electron-donating sites by the higher electron density of the carbon matrix. Hence, the ORR activity of BCNTs is due to that electron-deficient B can first attract the negatively charged O_2, further leading to an electron transfer from the carbon matrix to B. The higher electronic density can now be transferred to O_2 with B as a bridging atom, subsequently reduced to H_2O. Followed by these studies, a number of B-doped carbons are proposed to be reasonably active ORR catalysts. However, the

enhanced ORR active catalysts have been discovered when B is co-doped with other heteroatoms, especially with N. The synergistic effect of both B and N enhanced the ORR activity several folds.

With large atomic size and lower electronegativity, the P-doped carbons are also explored as ORR catalysts, by a defect-induced ORR mechanism. Lone pair electrons of P and empty 3d orbital shells can induce a large charge density difference in the carbon matrix and can accommodate the O_2 lone pairs, and thus P could also be a good choice as a dopant to carbon [91, 92]. Yang et al. [93] synthesized P-doped platelet-ordered mesoporous carbon (P-pOMC-800) as a metal-free ORR catalyst, with triphenylphosphine as a P source. The catalyst shows P–C and P–O bonding configurations in the XPS analysis. With 0.89 wt.% of P, the P-pOMC-800 catalyst shows excellent ORR activity, very close to that of the Pt/C catalyst, with a 3.8 number of electrons transferred per O_2 molecule, less than 5% of the peroxide yield (Fig. 2c). The other P-doped catalysts reported can be found in [94–96].

As stated earlier, due to the similar electronegativities of S and C, the effect of charge transfer and hence charge density is negligible in this system. However, it is found that the outer orbital mismatch between the S and C atoms can significantly change the spin densities. It is found that the S atom bonded covalently to the carbon and oxidized S which both can induce the spin density to the doped carbon, helping in catalyzing the ORR [21]. The S-doped atoms are located in the carbon matrix and S atoms in oxidized form; SO_2 formed at the zigzag edge are found to be ORR active. The carbon atoms with high spin density take a direct 4-electron transfer process [97]. Li et al. [98] synthesized sulfur-doped carbon nanotubes (p-SCNTs) by pyrolyzing the mixture of oxidized carbon nanotubes with p-benezenedithiol. The ORR analysis of the p-SCNTs annealed at 900 °C showed an excellent ORR activity as well as excellent tolerance to methanol in the alkaline electrolyte (Fig. 3a). Researchers also doped various halogens into the carbon materials and evaluated the effect of halogen-doped carbons on the ORR activity. For example, Jeon et al. [99] synthesized edge-halogen-derived graphene platelets (XGnPs = ClGnP, BrGnP, IGnP) by ball milling in the presence of chlorine (Cl_2), bromine (Br_2), and iodine (I_2), respectively. High-energy ball milling provides the desired kinetic energy to cleave the C–C bonds in graphite. This process generates active species like carbocations, carboanions, and carboradicals which interact with the halogens to give halogenated carbons. The synthesized XGnPs exhibit admirable ORR activity evaluated in the 0.1-M KOH electrolyte. Cyclic voltammetry studies indicate a distinct ORR curve in XGnPs ascertaining their intrinsic ORR activity in the order of IGnP > BrGnP > ClGnP. Similar conclusions were also drawn from linear step voltammetric studies, where IGnP gives a higher ORR activity along with excellent resistance to methanol species. The number of electrons transferred was found to be 3.5, 3.8, and 3.9 for ClGnP, BrGnP, and IGnP catalysts, respectively. However, as explained in the earlier sections, the ORR activity of the heteroatom-doped catalysts on the basis of electronegativity do not follow in the case of XGnPs, which seems to be contradictory to the doping-induced charge-transfer mechanism. According to the electronegativity concept, ClGnP should have delivered best ORR characteristics; however, in this case IGnP possesses a higher ORR activity. The higher ORR of IGnP could be related to the size of I, which is higher than Br and Cl, and hence the valance electrons of I are much easier to induce charge delocalization. Density functional theory calculations reveal that IGnPs bind with O_2 with a higher strength than BrGnPs (triplet state of free O_2 in the vacuum) and ClGnPs and hence the higher O–O bond length is observed in the case of IGnPs, favoring the O–O bond cleavage during ORR.

Zhan et al. [100] synthesized iodine- and N-doped graphene (ING) as a metal-free ORR catalyst by annealing graphite oxide with I_2 powder and NH_3 gas. It was observed that I and N were doped successfully into graphene. However, the amount of I doping is much less than that of N. The higher ORR activity for ING catalysts is observed than that of NG and IG catalysts, with a H_2O_2 of 7.4%. However, the ORR activity of ING catalysts is lower than the standard Pt/C catalyst. In another study, Yao et al. synthesized I-doped graphene by a thermal annealing of graphene oxide and iodine between 500 and 1000 °C. The ORR activity of I-graphene-900 shows similar activity to the Pt/C catalyst [101]. In another study, Jeon et al. synthesized I-doped activated carbon by ball milling of activated charcoal by iodine. However, the ORR activity of I-doped charcoal is much inferior to that of the Pt/C catalyst [102]. Ishizaki et al. [103] synthesized halogen-doped carbons by a solution plasma technique with benzene and halo benzenes (C_6F_6, C_6Cl_6, and C_6B_6) as carbon and halogen sources, and explored them as ORR catalysts. The contents of dopant levels were found to be 0.08, 0.09, and 0.06 at% for F, Cl, and Br dopants, respectively. This indicates that the solution plasma process induces very low doping contents of halogens compared with other solid-state synthesis protocols. This might be because of the low hydrogen abstraction capacity of the halogens, and it has the order of F-CNPS > Cl-CNPs > Br-CNPs. The XPS analysis shows the ionic and semi-ionic C–F bonds, C–Cl type of the covalent bond, and Br–C with ionic and two covalent bonds. In case of halogen-doped catalysts, it is found that the ionic and semi-ionic bonds are ORR-determining factors than the covalent bonds. This is because ionic bonds play a role of electrodonor and acceptor and help in the change transfer between C and halogens. The ORR activity of all the halogen catalysts synthesized in this study is much inferior to the Pt/C catalyst, when compared with the other halogen catalysts discussed above. This could be due to the very low doping contents of halogens. Authors in this study speculate that the general electronegativity rule of

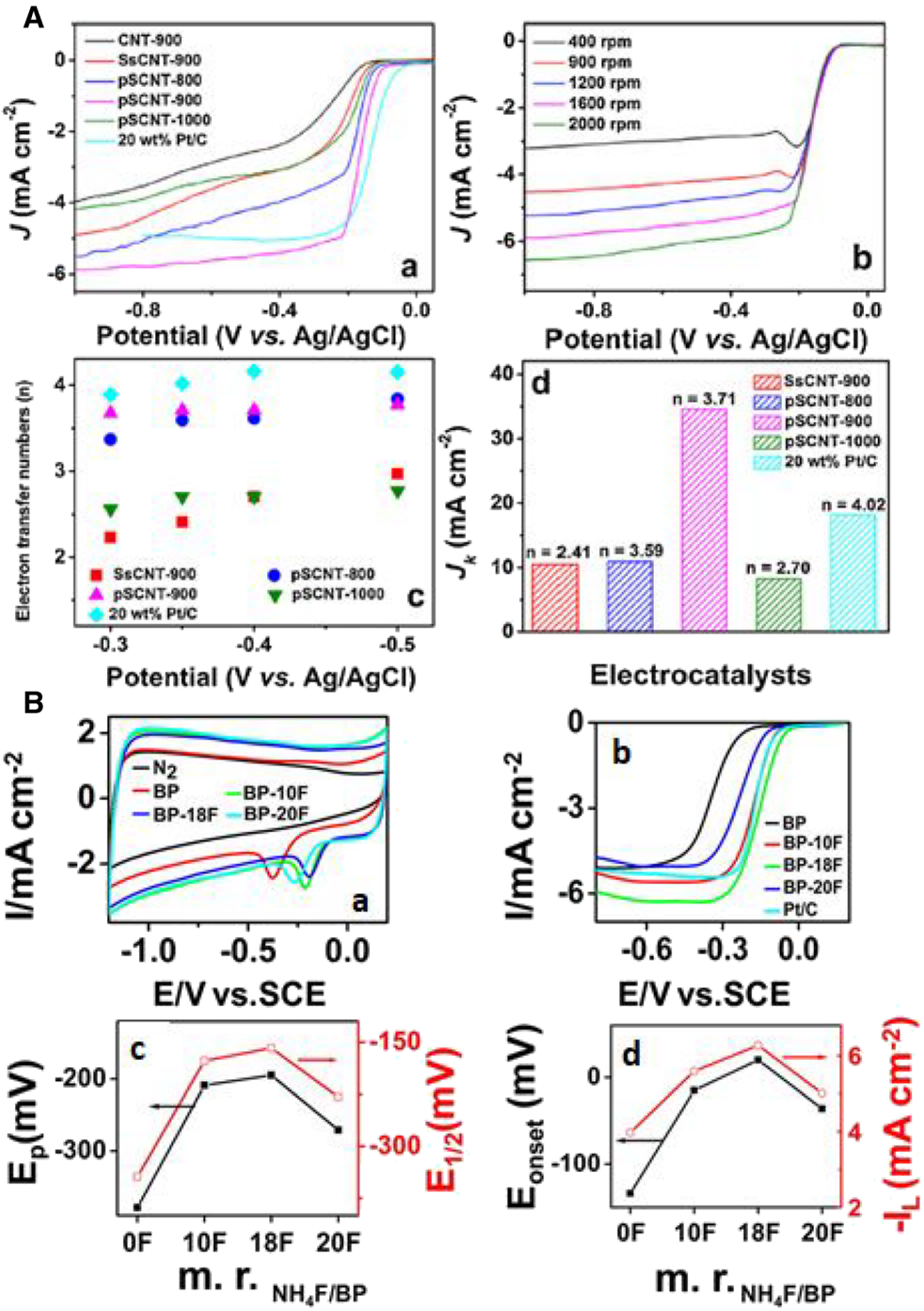

Fig. 3 **a** LSV curves for samples and Pt/C at 1600 rpm (a), and pSCNT-900 in O_2-saturated 0.1 M KOH aqueous solution with a sweep rate of 10 mV s^{-1} at the different rotation rates (b). The electron transfer number (n) of pSCNTs, SsCNT-900, and Pt/C at different potentials (c). Electrochemical activity for ORR given as the kinetic current density (J_k) at − 0.35 V for pSCNTs, SsCNT-900, and Pt/C (d) [98] Reprinted with permission from ref. 98 Copyright 2015 Elsevier. **b** (a) CV curves of BP-F catalysts in 0.1 M KOH with or without O_2. (b) Linear sweep curves of different BP-F catalysts and 20 wt% Pt in O2-saturated 0.1 M KOH with a rotation rate of 1600 rpm and a scan rate of 5 mV/s. The catalyst loading is 0.39 mg cm^{-2} for doped carbon catalysts and 0.12 mg cm^{-2} for commercial Pt/C. (c) Volcano-shaped dependences of E_p, $E_{1/2}$, E_{onset}, and (d) I_l on F doping [104] Reprinted with permission from ref. 104 Copyright 2013 American Chemical Society

explaining ORR activity may not suit for halogen-doped catalysts. There might be other factors such as bonding configuration and defects in carbon surface, which combinedly affects the ORR activity. However, further deeper investigations on the effect of halogens on ORR activity are needed to understand the mechanism of the ORR pathway.

Sun et al. [104, 105] reported F-doped carbon black (BP-F) as a metal-free ORR catalyst synthesized with NH_3F as the F source in alkaline and acidic electrolytes. It is observed that the ORR activity of BP-F increases with the increasing F content till 0.63 wt.%. The ORR activity of BP-18F shows 30 mV of the positive shift in the half-wave potential compared with the Pt/C catalysts in alkaline electrolytes, but still inferior to Pt/C in acidic electrolytes with a super low H_2O_2 percentage of < 0.1%. In addition, BP-18F catalysts show excellent tolerance to methanol and CO species in both acidic and alkaline electrolytes with excellent stability under potential cycling conditions. The authors claim that the semi ionic C–F bonds play a major role in the ORR process. It is observed that CB-F possesses higher O_2 adsorption energy along

with the large O–O and shorter C–O bond lengths. The natural bond orbital analysis results in a specific interaction between O orbitals and C orbitals in BP-F catalysts which activate the π orbital of C for enhancing ORR activity (Fig. 3b). Very recently, Zhang et al. [106] demonstrated a mechanochemical approach with a melamine hydrogen fluoride salt (MF salt), instead of the low boiling point NH_4F source, utilized in most of the F-derived catalysts. First, melamine hydrogen fluoride salt was obtained by an acid–base neutralization reaction between HF and melamine. HF is added to the aqueous solution of melamine and then the resulting solution was magnetically stirred and the water evaporated to obtain the MF salt, which was further heat-treated at 1000 °C to obtain NFC-1000. The decomposition temperature of MF salt is higher than that of NH_4F, preventing F loss at low temperatures, leading to the high F content of 1.52 at% relatively higher than the reported literatures. The resulting NFC-1000 catalyst showed an ORR onset potential of 0.82 V with an average number of 3.7 electrons transferred per O_2 molecule.

Dual-doped carbons as ORR catalysts

With this great motivation from the effect of monoatomic heteroatom-doped metal-free catalysts for ORR, researchers have developed various catalysts with two or more heteroatoms doped simultaneously into carbon, to utilize the synergistic effect of the different elements to further enhance the ORR activity in both acidic and alkaline electrolytes. Other heteroatoms include atoms with lower electronegativity values than carbon, such as B, P, and S, and higher electronegativity values than carbon, such as F, Cl, Br, and I [107].

It is also proposed that the doping of carbon nanomaterials with two heteroatoms, one with higher electronegativity and another with lower electronegativity, also enhances the ORR activity (Fig. 4a). This heterogeneity brings out special electronic properties to the carbon matrix favorable for many electrochemical redox reactions. In the N–B system, it is found that the B dopant weakens the O–O bond stretching and promotes the adsorption of OOH^-, to facilitate the oxygen reduction reaction [108]. A recent study by Kahan et al. [109] on B- and N-doped polycyclic aromatic hydrocarbons revealed that both N and B dopants' close proximity is very essential for ORR activity.

Qiao et al. [110] synthesized B,N-graphene and identified the ORR active B–C–N configuration and fundamentally explained the effect of B and N doping on the ORR activity. In this study, B,N-graphene was prepared by a two-step process, with no inactive by-product of the *h*-BN and *h*-BN/graphene hybrid, otherwise resulting in a single-step synthesis [111]. Further, they also propose the specific sequence of N and B doping to extract the best ORR characteristics of B,N-graphene. B doping was performed to the previously synthesized N-doped graphene which results in distinguishable C–N and B–C configurations. In this case, they found active pyridinic, pyrrolic, and graphitic-N configurations which also resulted in BC_3 configurations with no *h*-BN phase. The doping vice versa however resulted in lower N content and unwanted BC_2O and BC_3 configurations and hence lower electrocatalytic activity. The resulting B,N-graphene showed an enhanced cathodic ORR current density with a closer onset potential to the commercial Pt/C catalyst and singly doped B- and N-graphene catalyst. The number of electrons calculated from the K–L plot is found to be 3.97 for B,N-graphene with 98.5% of selectivity towards the 4-electron O_2 reduction process. Their DFT calculations suggest that B doping transforms "inactive" twofold-coordinated pyridinic N into "active". The DFT calculations also reveal the electronic configuration of a special B–C–N bond, where C atoms are first polarized by the effect of N. Further, charge transfer occurs from C to B atoms activating B atoms for ORR. This also signifies the importance of the C bridge. The configuration where B is directly bonded to N to give a BN configuration has a poor ORR activity due to the absence of bridging of C atoms.

Sun et al. [112] synthesized defect-rich, Zn template–derived, porous B- and N-doped carbons (B,N-carbon) from the thermal pyrolysis of ethyl cellulose and 4-(1-naphthyl)benzeneboronic acid in the NH_3 atmosphere. The synthesized catalysts show an excellent porous structure and high ORR activity and durability, similar to the Pt/C catalyst. First, the ethyl cellulose and 4-(1-naphthyl) benzeneboronic acid precursors were deposited onto the pre-synthesized Zn templates by a precipitation method, and then the whole mixture was subjected to pyrolysis in the NH_3 atmosphere. The porosity to the carbon matrix originated from the thermal evaporation of the Zn template into ZnO. The defect structure to the carbon surface is induced by the decomposition of ethyl cellulose which contains oxygen atoms, into CO_x and H_2O. The interconnected Zn hydroxide nanosheet template is delivered to the carbon structure as the template decomposes during the pyrolysis process, simultaneously giving an ordered structure and porosity to carbon. The ORR activity of B,N-carbon is found to be equal to the Pt/C catalyst, with an onset potential of 0.98 V and half-wave potential of 0.84 V, which is 17 mV above the standard Pt/C catalyst, indicating the promising nature of B,N-carbon. Moreover, B,N-carbon also shows excellent stability over 80 h in the chronoamperometric test with a loss of only 18% of the relative current compared with 48.3% of loss for the Pt/C catalyst. B,N-carbon also shows a higher performance in OER more than the standard RuO_2. Due to its excellent ORR and OER activity, B,N-carbon is utilized as an anode and cathode catalyst for Zn-air-rechargeable batteries, where it shows excellent charging and discharging polarization curves better than the Pt/C + RuO_2 catalyst.

Recently, Wang et al. synthesized porous boron nitride nanosheets (BCNs) as an efficient ORR catalyst in both acidic

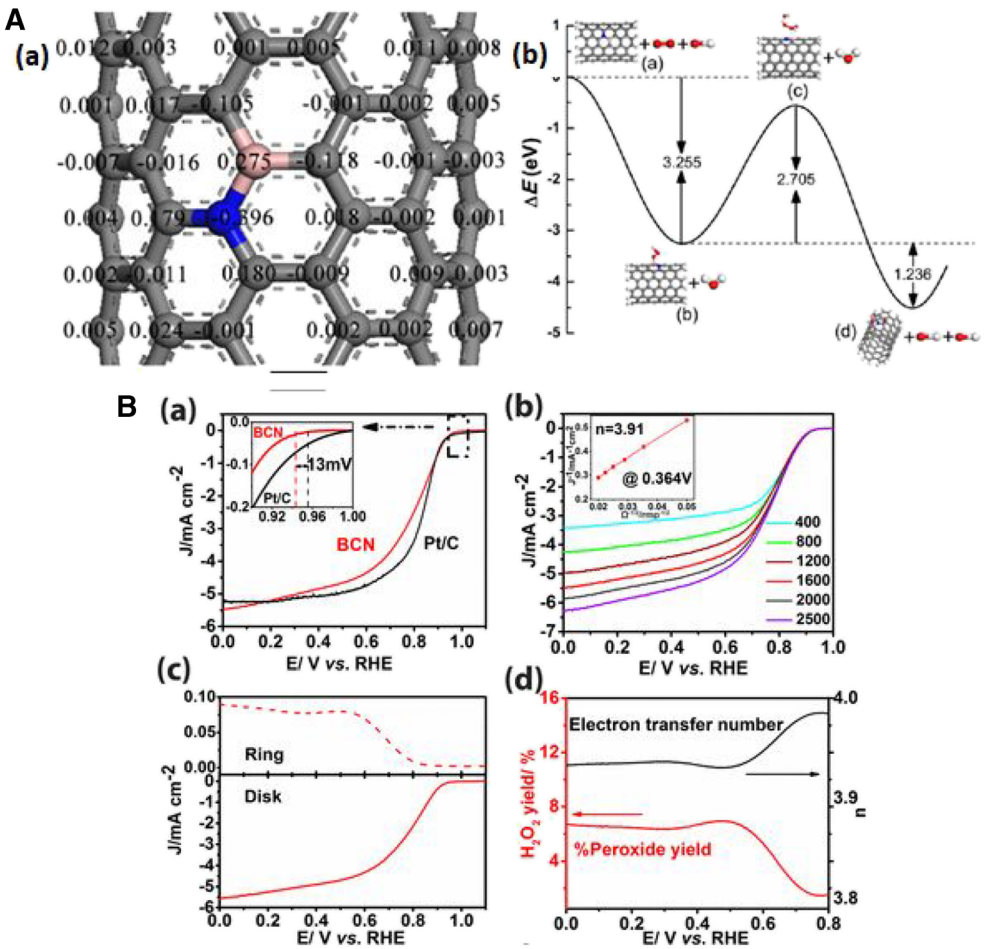

Fig. 4 **a** (a) The calculated Mülliken charge distribution for the N,B-CNT. The blue ball is the doped nitrogen atom, the pink ball represents the doped boron atom, and the gray balls are carbon atoms. (right). (b) Schematic representations of possible reaction patterns on the surface of N,B-CNT [108] Reprinted with permission from ref. 108 Copyright 2016 Elsevier. **b** (a) ORR catalytic performance of the porous few-layered BCN in 0.1 M KOH. (a) LSV curves of BCN catalysts and Pt/C at a rotation rate of 1600 rpm and a scan rate of 5 mV/s. The inset shows the higher magnification of LSV curves between 0.9 and 1.0 V vs. RHE. (b) LSV curves of BCN catalysts with various rotation rates from 400 to 2500 rpm at a scan rate of 5 mV/s. The inset shows the corresponding Koutecky–Levich plot. (c) RRDE voltammograms and (d) H_2O_2 yield corresponding to the total oxygen reduction products and the calculated electron transfer number of few-layered BCN [113] Reprinted with permission from ref. 113 Copyright 2017 American Chemical Society

and alkaline electrolytes [113]. The BCN is synthesized by a sol-gel synthesis process. XPS analysis shows a successful B–C–N bonding configuration implying the presence of ORR active centers in the catalyst. The ORR activity of BCN catalysts was found to be excellent, with an onset potential of 0.940 V, with a 3.91 number of electrons transferred per O_2 molecule. The H_2O_2 percentage was found to be below 6%, suggesting a direct 4 e^- reduction reaction of the O_2 molecule. The enhanced ORR activity of BCN is due to the high concentration of pyridinic N, which can enhance the adsorption of O_2 to the adjacent Lewis-based carbon atoms for its subsequent reduction to water. Existence of a higher proportion of B–N–C bonding configurations, in contrast to the ORR inactive BN configuration, is also a reason for the higher ORR activity of the BCN catalyst. Furthermore, it is also found that the presence of B–O-ionizable bonds could enhance the hydrophilicity to the catalyst active sites, enhancing O_2 availability (Fig. 4b). Other notable reports on N and B carbons can be found in [114–116].

For example, Dai et al. [13] synthesized N- and P-doped multiwalled carbon nanotubes by a CVD with ferrocene, pyridine, and triphenylphosphine as precursors (NP-ACNT). It is proposed that the co-doping of N and P creates highly localized states at the Fermi level. The NP-ACNT catalyst shows pyridinic-N and graphitic-N along with P incorporated into the carbon matrix (P–C). The NP-ACNT catalyst showed enhanced ORR activity at a similar loading with the Pt/C catalyst with 3.67–3.88 number of electrons transferred with a potential ranging from − 0.3 to 0.6 V vs Ag/AgCl reference electrode. Woo et al. [117] synthesized P and N dual-doped carbon with dicyandiamide (DCDA), phosphoric acid, 900 °C, under an Ar atmosphere in the presence of Fe and Co catalytic centers. NPDC-10 catalysts showed a more positive ORR onset potential of 0.6 V (vs. Ag/AgCl) in the acidic electrolyte with enhanced capacitance values coupled with the large surface area of NPDC-10. The ORR activity of NPDC-10 is higher than the NDC catalyst by 50 mV vs. Ag/AgCl, indicating the synergistic effect of N and P towards ORR. In addition to the enhancement in ORR activity, P doping also signifies the changes in the morphological effect on the catalysts. The NDC catalyst shows a horn-type carbon structure; however, when P co-doped together with N doping, the horn-type carbon structure changes to the crumple's graphene sheets. This conversion factor depends on the content of P doping in

NPDC-10. It is observed that the NPDC-10 catalyst shows many wrinkled and uneven graphene sheets. When there are further increases in the content of P, wrinkled graphene sheets converted into graphene lumps. This indicates that P doping not only enhances ORR activity but also has a structural transformation role. In addition to the synergistic effect of N and P or in principle any two different heteroatoms, the surface area and porosity of the carbon catalysts are also playing an important role. Recently, Sun et al. [118] synthesized an N and P dual-doped porous aerogel carbon catalysts by hydrothermal synthesis process. Surfactant-assisted self-assembly of phytic acid and pyrrole with P123 results in N, P hydrogel NPH, which was freeze-dried, followed by CO_2 activation which gives NPPC. The resulting NPPC catalyst shows an onset potential of 0.90 V, and a half-wave potential of 0.81 V vs RHE, much higher than the Pt/C catalyst (5 wt.%), with an average of 3.88 electrons transferred for a single O_2 molecule. High pyridinic-N and graphitic-N and a synergistic effect of N and P create defects which in turn modify the surrounding carbon atoms, thus enhancing the ORR activity. In addition, high porosity created by CO_2 activation provides adequate oxygen reaching towards the ORR active sites. In another recent study by Li et al. [119], highly active N- and P-doped porous carbon nanosheets (N,P-CS) are synthesized with the pyrolysis of the mixture of glucose, phosphorous acid, melamine, and montmorillonite mixture. The N,P-CS catalyst showed a high surface area and a mixture of mesopores and micropores. The ORR activity of the N,P-CS catalyst is found to be more positive than the Pt/C catalyst, with 20 and 30 mV higher in onset and half-wave potential in the alkaline medium. The peroxide yield was calculated to be between 3 and 5%, suggesting a dominant 4-electron reduction process on the N,P-CS catalyst. Moreover, in acidic media the N,P-CS catalyst shows an appreciable ORR activity with just 62 mV lesser than the Pt/C catalyst.

In dual-doped carbons, a lot of attention is paid towards co-doping of N with S, as S doping is found to be easier to replace the carbon when N is doped along with it [120, 121]. For example, Qu et al. [122] synthesized N, S-doped carbon nanosheets with polydopamine and 2-mercaptoethanol as N and S sources, respectively. The N,S-CN-doped catalyst shows excellent ORR activity with a high ORR onset potential and low Tafel slope, when compared with the N–CN-doped catalyst, suggesting that the co-doping of N and S could enhance the ORR activity. The asymmetrical spin and charge densities of the carbons, due to N and S doping, enhances the ORR adsorption and reduction to water. Moreover, the excellent mesoporous structure of the catalysts enhances the mass diffusion and electrochemical double-layer capacitance, suggesting that the N,S-CN catalyst possesses an excellent surface area with abundant active sites.

Generally, the doping process includes mixing of the functionalized carbons with a large amount of precursors with respect to carbon, followed by a pyrolysis process at higher temperatures. Though the pyrolysis process effectively introduces the heteroatoms, it also leads to the release of a large amount of toxins by gaseous by-products especially during the synthesis of sulfur-doped carbons. Arunchander et al. [123] synthesized N-S/Gr catalysts by a mild and in situ chemical polymerization of 6-N,N-dibutylamine-1,3,5-triazine-2,4-dithiol on graphene sheets. The resulting N-S/Gr catalyst showed enhanced ORR activity with an ORR onset potential of 0.92 V vs RHE with an average electron transfer of 3.7. The N-S/Gr catalyst showed enhanced stability in both potential cycling and potentiostatic tests when compared with the Pt/C catalyst. Moreover, the N-S/Gr catalyst also delivered a 20 mW cm^{-2} power density in a single AEMFC, but the power density is still inferior to that of Pt/C catalysts. On the other hand, ionic liquid–derived catalysts are also proposed as efficient electrocatalysts. For instance, Wu et al. [124] synthesized a three-dimensional ordered macroporous nitrogen and sulfur co-doped carbons with an liquid (IL) bearing crosslinkable alkynyl groups, i.e., [1-methyl-3-propagylimidazolium bromide] [bis (trifluoromethyl)sulfonyl imide] ([MPIm][Tf2N]). The resulting IL catalysts showed excellent N- and S-doped electrocatalyst with a three-dimensional ordered macrospore structure with an average pore size of 5 nm and a BET surface area of 1104 m^{-2} g^{-1}. The IL derived 3DOM NS-C-1100 catalysts showed outperformed ORR characteristics over Pt/C catalysts with an onset potential of ~ 0.11 V vs Hg/HgO when compared with Pt/C which was ~ 0.10 V vs Hg/HgO. Such an enhanced ORR activity is due to the well-ordered three-dimensional mesoporous structure which enhances the exposure of the doped active sites and also enhances the mass transport kinetics towards the electrode–electrolyte interface. Other catalysts derived from ionic liquids can be found in [125, 126].

It seems that the single I-doped carbons did not possess good ORR activity. However, when I is doped together with N, the activity of the synergistic catalyst is found to be several folds higher than the single I-doped carbons. For example, Zhan et al. [127] synthesized iodine- and N-doped carbon (ING) by a thermal annealing of I and NH_3. Electrochemical measurements revealed that the ING catalyst showed enhanced ORR activity with the onset potential of 0.945 V equal to the Pt/C catalyst with 7.4% of H_2O_2. Interestingly, the ING catalyst also shows good ORR activity in the acidic electrolyte with a 105-mV less half-wave potential than the Pt/c catalyst in 0.1 M $HClO_4$. In another study, Liu [128] synthesized a highly efficient I- and N-doped carbon by a hydrogen-bonded organic framework, which shows excellent ORR activity similar to the Pt/C catalyst. Moreover, the I-doped carbons are also utilized as a high-performance catalyst in membrane electrode assemblies [129, 130]. Though the I-doped carbons posses inferior ORR activity to that of Pt/C, when I is doped together with other heteroatoms such as N and S, I-doped carbons showed enhanced ORR activity. This could be due

to the synergistic effect of I and other heteroatoms. Moreover, synergistic interactions could also enhance the conductivity of carbon, which was believed to be the responsible factor for the enhanced ORR activity [131, 132].

In another study, Sun et al. [133] synthesized N and F co-doped carbon blacks as methanol-tolerant cathode catalysts in alkaline direct methanol-tolerant fuel cells (ADMFC). The BP-2000NF catalyst showed excellent tolerance to the method in comparison with the traditional Pt/C catalysts. In ADMFC configuration, BP2000-NF exhibited 15 mW cm^{-2} power density at 60 °C, compared with 13 mW cm^{-2}, with almost no change in its voltage recorded after 24 h at the constant current of 200 mA. The enhanced ORR activity of BP2000-NF is attributed to the high content of ionic and semi-ionic C–F bond configurations along with pyridinic-N and pyrrolic-N configurations. Density functional theory calculations show the lowest band gap of CB–NF than CB–N, CB–F, and CB and after the O_2 adsorption the O–O bond lengths increase from 1.241, 1.254, and 1.28 for CB–N, CB–F, and CB–NF, respectively. This indicates the specific synergistic interaction of N and F towards ORR.

Peera et al. [134] synthesized N- and F-doped graphite nanofibers as a high-durability ORR catalyst evaluated in the acidic electrolyte (0.5 M $HClO_4$). The synergistic effects of the N and F heteroatoms are assessed by enhanced ORR activity of the N-F/GNF catalyst over N-GNF and F-GNF catalysts. In the acidic electrolyte, the N-F/GNF catalyst showed a half-wave potential of 0.63 V and redox peak at 0.50 V (Fig. 5a). The N-F/GNF catalyst also shows extraordinary stability in the acidic electrolyte (20,000 potential cycles) and tolerance to methanol and CO species. XPS analysis of the N-F/GNF catalyst showed a high content of pyridinic-N and ionic and semi-ionic C–F bonds (Fig. 5b). Moreover, the N-F/GNF catalyst was also evaluated in a single-cell fuel cell device, which delivered a 165 mW cm^{-2} power density in the H_2-O_2 fuel cell with a cathode catalyst loading of 2 mg cm^{-2}. The authors also conclude some of the important points not discussed by the authors of previously reported F-doped carbons. The authors propose a site specificity of the F atoms in the vicinity of N doping and the effect of F doping on the structural transformation of the carbon nanostructures. F doping structurally transforms graphitic nanofibers (GNF) into graphene structures, ascertained from the density functional theory calculations. From the by-layer model studies, it is proposed that F doping increases the interlayer space between the two layers to a greater extent and the perpendicular occupation of the F atoms forces the two layers to be apart and hence induces the strain in the nanofibers, converting them into graphene structures. Their DFT calculations also propose that F cannot form a bond with C from either forms of the C–F configurations, in the absence of at least one N atom in the vicinity. In the absence of N in the vicinity, F atoms can only intercalate between the layers, but cannot form C–F bonds, and hence C–F bonds can only be realized in the N-doped carbons. Moreover, their DFT calculation also reveals a specific doping site of F in the N-doped carbons. With the graphitic-N-type configurations, F atoms form a bond with the immediate C atom (first nearest neighbor (FNN) C atoms), whereas with the pyridinic-N-type configurations, F atoms form a bond with the second C atom (second nearest neighbor (SNN) C atoms) derived from the Bader charge analysis as shown in Fig. 5c. The developed N-F/GNF catalyst was also evaluated as a cathode catalyst in a real fuel cell atmosphere, where it delivered 160 mW cm^{-2} power density. In another, a similar concept of F doping–induced unzipping was also ascertained by Srinu Akula et al.'s [135] study by utilization of MWCNTs, where MWCNTs convert into graphene sheets with the enhanced ORR activity. However, a better understanding of the effect of F doping on the ORR, the synergistic interactions of F with other heteroatoms, the effect of individual C–F configurations (ionic, semi-ionic, and covalent C–F), and their possible existence in the presence or absence of other heteroatoms are still lacking and are open to future discussion in literatures. It is also proposed by Wood et al. [136] that F doping not only enhances ORR activity but also increases the stability to carbons, proposed from a model carbon study. This was experimentally proved by Peera et al. [137, 138].

Fu et al. synthesized nitrogen and fluorine-co-doped carbon nanowire aerogels (NFCNAs) as metal-free electrocatalysts from tellurium nanowires as hard templates and applied them as oxygen reduction catalysts [139]. Previously synthesized Te nanowires and glucose solution were hydrothermally treated, and the resulting Te nanowire hydrogels were immersed in NH_4F solution and then subsequently pyrolysis at 1000 °C leading to the formation of graphitized NFCNAs and subsequent decomposition of the Te template. NFCNAs show nanowire structures similar to base Te nanowires. NFCNAs show the N and F contents of 1.8 and 0.04% (atomic) with large proportions of graphitic-N and ionic C–F and semi-ionic C–F configurations, with a higher ratio of ionic C–F bond (69%). NFCNAs-18–1000 shows a higher ORR onset potential and half-wave potential of 0.912 and 0.825 V which are highly comparable with that of state-of-the-art Pt/C catalysts, 0.934 and 0.844 V vs RHE. The number of electrons transferred per O_2 molecule was found to be 3.7 for the NFCNAs-18–1000 catalyst. Similar results were also found on N-F/rGO by Qiao et al. [140].

As it is known that doping of F into the carbon matrix is difficult, usually a large amount of the F source is utilized, and in most cases, it is NH_4F in mass ratios as high as 20 times that of carbon. Besides, the easy decomposition of NH4F at relatively lower temperatures possesses an additional synthetic problem to enhance the doping levels of Gong et al.'s [141] synthesized N, F-co-doped microporous carbon nanofibers (N, F-MCFs) as efficient ORR catalysts in the 0.1-M KOH electrolyte.

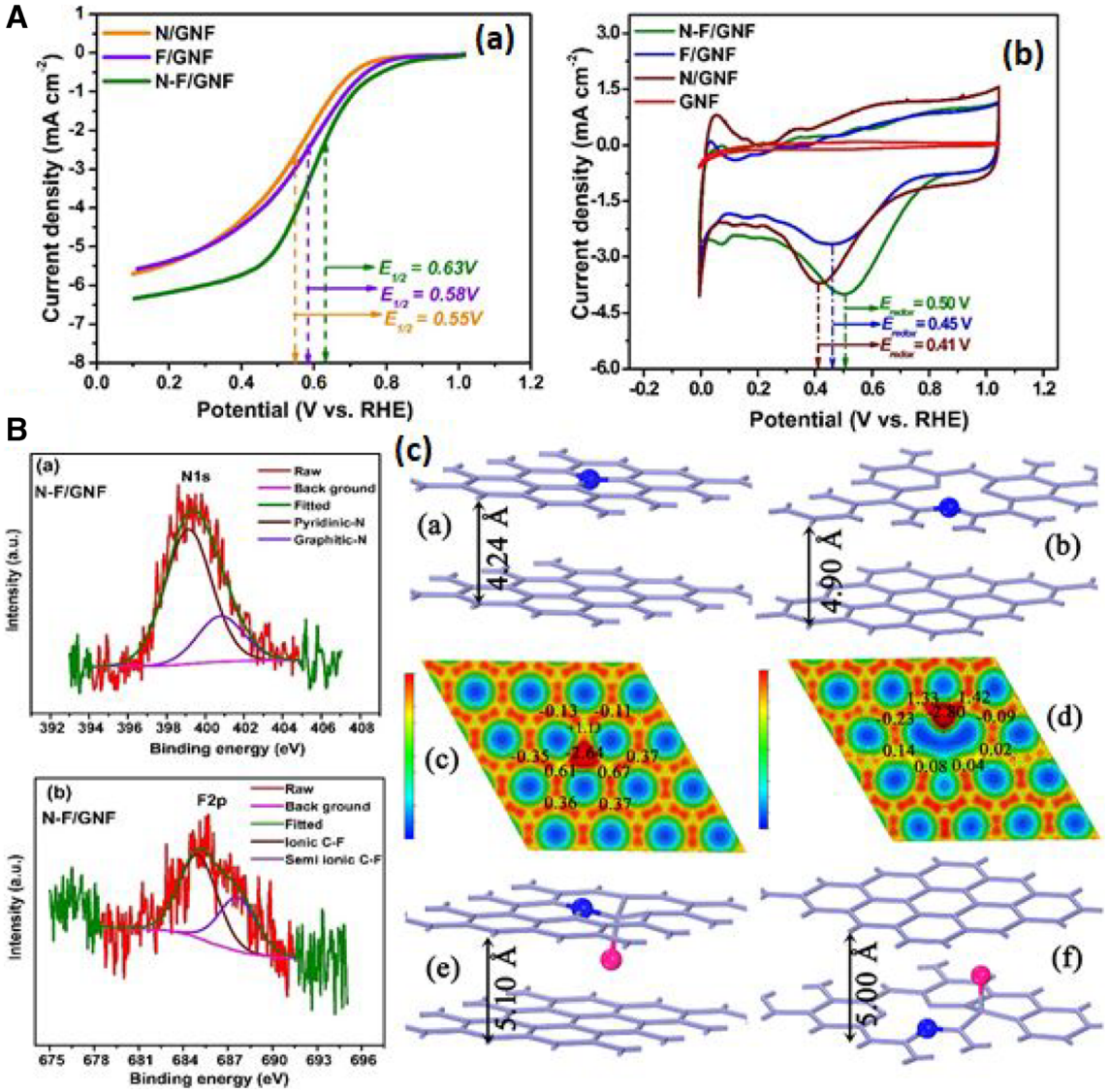

Fig. 5 **a** (a) The LSV curves of N/GNF, F/GNF, and N–F/GNF catalyst recorded at 1600 rpm in a N_2,O_2-saturated aqueous solution of 0.5 M $HClO_4$ at a scan rate of 5 mV s^{-1}. (b) Cyclic voltammograms for GNF, N/GNF, F/GNF, and N–F/GNF catalysts in O_2-saturated aqueous solution of 0.5 M $HClO_4$ at a scan rate of 50 mV s^{-1}. **b** Deconvoluted XPS spectra for (a) N1s and (b) F2p of the N–F/GNF. **c** Stick models of optimized A–A stacked (a) GRN- and (b) PYN-doped Gr bilayers are depicted with their respective charge density contours in (c, d), and the stick models of F co-doped models of GRN and PYN are shown in (e, f). N and F atoms are represented as blue- and pink-colored balls (Counter values are given inset. Bader charges of selected atoms are also given.) [134] Reprinted with permission from ref. 134 Copyright 2015 Elsevier

A tri-component polymer mixture composed of polyacrylonitrile (PVN)/polyvinylidene fluoride (PVDF)/polyvinylpyrrolidone (PVP) (PAN/PVDF/PVP) is electrospinned, followed by carbonization which yielded a N, F-MCF electrocatalyst. Carbon and fluorine are derived from PVDF, and PAN serves as a C and N source, whereas PVP is utilized as a porogen. The resulting N, F-MCFs show a porous carbon nanofiber with a decent graphitization. XPS analysis shows F atomic percentage as high as 2.86%, much higher than the earlier reports, which could enhance the ORR activity in a greater extent. High-resolution F spectra show three uniquely deconvoluted peaks, ionic-F (685.4 ± 0.2 eV), and two different types of semi-ionic-F bonds, namely, CH_2-CF_2 and CHF-CHF, at 689 ± 0.2 eV and 687.2 ± 0.2 eV, respectively. These two types of semi-ionic bonds have not been observed before, which might be due to the low content of F in other reports. The authors in this study attribute ionic F bonds as responsible for the improved electronic conductivity and catalytic activity of N, F-MCFs-A, though the role of semi-ionic C–F bonds needs to be solved for their role in catalytic activity. The ORR activity of the N, F-MCFs-A catalyst shows an onset potential of 0.94 V vs RHE, with a half-wave potential of 0.81 V, much closer to the commercial Pt/C catalyst half-wave potential of 0.83 V vs RHE.

Tri-doped/multi-heteroatom doped catalysts

It is known from the dual-doped carbon catalysts that the presence of two different heteroatoms can synergistically improve the ORR activity. Research was also conducted by doping three or more different metals to extract the maximum activity from the heteroatoms. For instance, Tao et al. [142] synthesized a N, P, S tri-doped catalyst (NPSCS) with phosphazene, as a N and P source and sulponyldipehon as a C and S source. A DFT calculation of N, P, S co-doped carbon revealed that a large difference in charge density of the carbon atoms is observed on N, P, S co-doped graphene, compared with the N and S-doped graphene, due to the electron accepting nature of the P atoms. Hence, it is concluded that P doping regulates the overall change density in the N, P, S tri-doped catalyst. NPSCS catalysts show an ORR onset potential of 0.965 V and a half-wave potential of 0.834 V, comparable with the Pt/C catalyst, with a lowest Tafel slope of 50.6 mV dec^{-1}. In contrast to this study, the effect of S on the enhancement of N, P co-doped carbon has been established by Zan et al. [143] in which the N, P-3D hierarchically porous carbon catalyst is co-pyrolyzed with thiourea to generate the S, N, P-HPC electrocatalyst. With 4.35, 2.96, and 1.29 at% of N, P, and S, the S, N, P-HPC electrocatalyst ORR activity surpasses the commercial Pt/C catalyst in 0.1 M KOH. Interestingly, the ORR activity of N, P-doped carbons was found to be lesser than the S, N, P-HPC electrocatalyst, clearly indicating the definite role of S in enhancing the ORR activity. The ORR activity of the S, N, P-HPC electrocatalyst is also evaluated in 0.1 M $HClO_4$. In acidic electrolytes, the S, N, P-HPC electrocatalyst shows an admirable ORR activity, again much higher than the N, P-HPC catalyst, but with lower ORR activity than the Pt/C catalyst. XPS and XANES analysis reveals that the ORR activity of the S, N, P-HPC electrocatalyst is related with the ratio of S_{red}/S_{ox} species. The possible S_{red} species would be –C–S–C– and –C=S– configurations, which could play a vital role in redistributing the spin density of the surrounded carbon atoms and thus lower the energy barrier for the adsorption of O_2. From the above two studies, it is clear that the doping of S and P could certainly enhance the overall activity of the N-doped carbons. Other similar tri-doped systems investigated are, N, S, P tri-doped graphene [144] and N, S, P tri-doped carbon nanosheets [145, 146].

Zhang et al. [147] synthesized a tri-doped graphene catalyst composed of N, P, and F which was obtained by thermal pyrolysis of ammonium hexafluorophosphate (NH_4PF_6) and polyaniline-coated graphene oxide as the precursors of N, F, and P and successfully applied the tri-doped catalyst (GO-PANi-FP) for electrocatalytic oxygen reduction (ORR) and evolution (OER) and hydrogen evolution reactions (HER). The thermal decomposition of the inorganic precursor NH_4PF_6 also acts as a porous template, in addition to the source of N, F, and F, by the evolution of gaseous products during the heat treatment process. The resulting GO-PANi-FP catalyst showed excellent electrochemical properties due to the synergistic effect of the dopants (N, P, and F) on charge/spin densities of the adjacent C atoms, together with the porous structure of the catalyst. XPS analysis shows the existence of N, P, and F dopants with 7.11, 0.37, and 0.33 at%, respectively. Accordingly, the GO-PANi31-FP catalyst showed excellent ORR activity. However, the activity of the GO-PANi31-FP catalyst is still lower than the commercial Pt/C catalyst by 40 mV. To add additional information, the GO-PANi-FP catalyst showed excellent OER activity comparable with the RuO_2 catalysts. At the current density of 10 mA cm^{-2}, the GO-PANi-FP catalyst shows similar overpotential with that of the RuO_2 catalyst. This indicates that the GO-PANi-FP catalyst is a promising catalyst for OER. Doping of B to the N and F dual-doped catalysts is also proposed. Wang et al. [148] synthesized N, F, and B tri-doped carbon nanofibers (TD-CFs) by electrospinning polyacrylonitrile and tetrafluoroborate in dimethylformamide solution. The TD-CFs catalyst shows clear distribution and doping of N, B, and F atoms. The TD-CF catalyst shows enhanced ORR activity than the catalyst synthesized without boron, suggesting the encouraging effect of boron in the catalyst. In another study by Liu et al. [149], the N, S, B tri-doped CNT catalyst is synthesized; the ORR activity of N–S–B CNTs is found to be very close to the commercial 20 wt.% Pt/C catalyst with 3.98–4.05 electrons transferred per O_2 molecule. By comparing the N, F, and B system with the N, S, and B system, the later system seems to be more active than the former system.

Van Pham et al. [150] proposed a multi-heteroatom-doped carbon nanotube catalyst (MH-CNT) as an efficient ORR catalyst in the alkaline medium. The oxidized/unzipped CNTs were doped with S by refluxing with P_4S_{10} in dimethylformamide (DMF) at 150 °C. Further doping of N and F was performed by Nafion and DMF at 600 °C, where F and N radicals are formed and act as dopants to the CNT to give MH-DCNT600. When MH-DCNT600 was subjected to higher temperatures of around 800 and 1000 °C, it is observed that the F atoms are vanished from the catalysts as evident from XPS analysis. The authors claim that the F atoms are removed in the form of carbon monofluoride at the temperatures of above 500 °C. This process takes away the C atoms from the CNT matrix and hence creates carbon-vacant defects in the CNTs. This claim seems to be slightly contradictory as other authors prepare F-doped carbons at temperatures above 900 °C (discussed in later sections). Accordingly, in their studies, MH-DCNTs-800 showed enhanced ORR activity with the E_{onset} of 0.91 V vs RHE, over S-DCNT150 (E_{onset} of 0.85 V vs RHE) with an average electron transfer number of 3.5 and 90% of the ORR process by a dominant 4-electron transfer. The authors also demonstrated the activity of MH-DNCT-800 in alkaline fuel cell atmospheric conditions, which delivered a peak of 250 mW cm^{-2} and open-circuit voltage of 0.9 V.

Recently, Srinu et al. [41] synthesized N, S, and F tri-doped carbons as an excellent ORR catalyst in both acidic and basic electrolytes. The pyrolysis of the sulfonated polyaniline–doped ketjenblack carbon in the presence of ammonium fluoride yields a N, S, F tri-doped catalyst (N–S–F/KB). The N–S–F/KB catalyst showed excellent ORR activity, over dual-doped N–S/KB catalyst. The N–S–F/KB catalyst shows 50 mV and 180 mV higher half-wave potential, than the dual-doped N–S/KB catalyst, in alkaline and acidic electrolytes. This clearly indicates the synergistic effect of F on the enhancement of ORR activity. Further, it also suggests that the addition of F doping is one of the effective strategies to enhance the ORR activity in an acidic electrolyte. Moreover, the N–S–F/KB catalyst also shows excellent durability with 20-mV loss in half-wave potentials in both acidic and alkaline electrolytes, after 10,000 potential cycles. Furthermore, the peroxide yield is found to be much lower for the N–S–F/KB catalyst than the N–S/KB catalyst, suggesting a definite role of F on the ORR mechanism.

As a short conclusion from the heteroatom-doped catalysts, irrespective of the doped atom, it is found that all the doped catalysts show enhanced ORR activity. Among them, the N-doped catalysts alone can show high ORR activity in alkaline and acidic electrolyte. In all other cases, the doped carbon activity is highly dependent on the synthesis of the catalyst, dopant content, and dopant configurations. However, when the dopants are co-doped with other elements, especially with N atoms, many studies found that the ORR activity has enhanced several folds. It seems that in all the dual-doped, ternary-doped, or multi-doped heteroatoms, the presence of N seems to be essential and vital for the oral enhancement effect. Very recently, Preuss et al. [151] drew similar conclusions that N doping was only exerting the actual influence on the electrocatalytic activity, while other dopants possibly assisted the N-doped carbon to enhance the overall ORR activity, but N plays a prime central role.

Metalloid catalysts

In recent years, metalloid-doped catalysts were utilized for ORR. The metalloids are those elements whose chemical properties are intermediate with the metal and nonmetals. The investigated metalloid elements are Ge, Si, Sb, and As. In search of metalloids, dopant germanium (Ge) has attracted much attention because of its special properties such as semiconductor, high carrier mobility, and 10,000 times higher conductivity in comparison with Si, and it can be easily doped into the carbon materials [152–154]. Ge also has a similar electronic configuration with C, and it also has high injection velocity [155]. Ge has an electronegativity (2.01) less than carbon (2.55) which can also be a good choice of dopant to the carbon matrix which can modify the electronic configuration of carbon to impart the electrocatalytic properties. However, Ge alone did not meet the standard ORR activity as Pt and hence it was co-doped in combination with doping of heteroatoms like N, S, and P.

Wang et al. [156] synthesized a hybrid catalyst of Ge and N-doped carbon nanotubes (Ge-CNTs and GeN-CNTs) and evaluated their ORR activity in the 0.1-M KOH electrolyte. The Ge-CNTs and GeN-CNTs were synthesized by a pyrolysis process with hydrogen gas, tetraethyl germanium, and aniline sources over $FeMo/Al_2O_3$ as a catalyst. 3d XPS spectra of Ge in GeN-CNTs3 show a pronounced Ge–C bond at 31.4 eV. It is also observed that the Ge-CNT catalysts possess a higher ORR activity compared with the pure CNT, which indicates a definite role of Ge doping towards ORR activity. Further enhancement in ORR activity is observed for GeN-CNTs3 with the enhanced number of electrons transferred from 3.0 (N-CNT) to 3.86 (GeN-CNTs3). Their DFT calculations suggest that Ge doping turns the neighboring neutrally charged carbon atoms into negatively charged with substantial decreases in the energy gap of HOMO to LUMO, and hence Ge was proven to be an effective dopant to modify the electronic properties of the carbons. She et al. [157] reported N–Ge–CNTs as a ORR catalyst by a one-pot synthesis of multiwalled CNTs in the presence of carboxyethyl germanium sesquioxide as a Ge source and NH_3 atmosphere as a source of N. Transmission electron microscopy and XPS analysis of N–Ge–CNTs shows the successful incorporation of Ge and N into the CNT. Especially, Ge 3d spectra show four distinguishable peaks for metallic Ge, Ge–C, Ge–Nx, and Ge–O at 29.9, 30.9, 31.4, and 32.0 eV, respectively. Further, the N spectra also show Ge-N binding configuration at 398.2 eV, other than the usual pyloric and pyridinic N species. These results convincingly indicate that the existence of Ge–N–C active species is similar to the M–N–C active sites proposed earlier by different research groups. Further, N–Ge–CNTs-2 catalysts show a higher ORR onset potential than the CNTs (− 0.16 V), Ge–CNTs-2 (− 0.16 V), and N–CNTs (− 0.10 V vs AG/AgCl) electrodes, which indicates that Ge and N doping effectively enhances the ORR activity. The N–Ge–CNTs-2 catalyst also effectively catalyzes the ORR reaction by a dominant electropathway as determined by the 3.94 number of electrons transferred per O_2 molecule, with below 10% of H_2O_2 production (Fig. 6a). In spite of this, the overall ORR activity of N–Ge–CNTs still underperforms the Pt/C catalysts in the alkaline electrolyte. The work function analysis of the various possible structures of Ge–N–C by DFT calculations indicates that the existence of GeN_4 and NC_3 configurations effectively reduces the work function of the ORR intermediates from 4.19 eV (CNT) to 3.78 (NC_3) and 3.63 eV (co-existence of GeN_4 and NC_3 configurations) indicating the definitive role of N and Ge doping towards ORR (Fig. 6b). Investigations on the combination of Ge with N- and P-doped carbons (Ge-NCNTs-2 and Ge-P-CNTs-2 certainly enhances the ORR activity, but still the work function of these catalysts is not

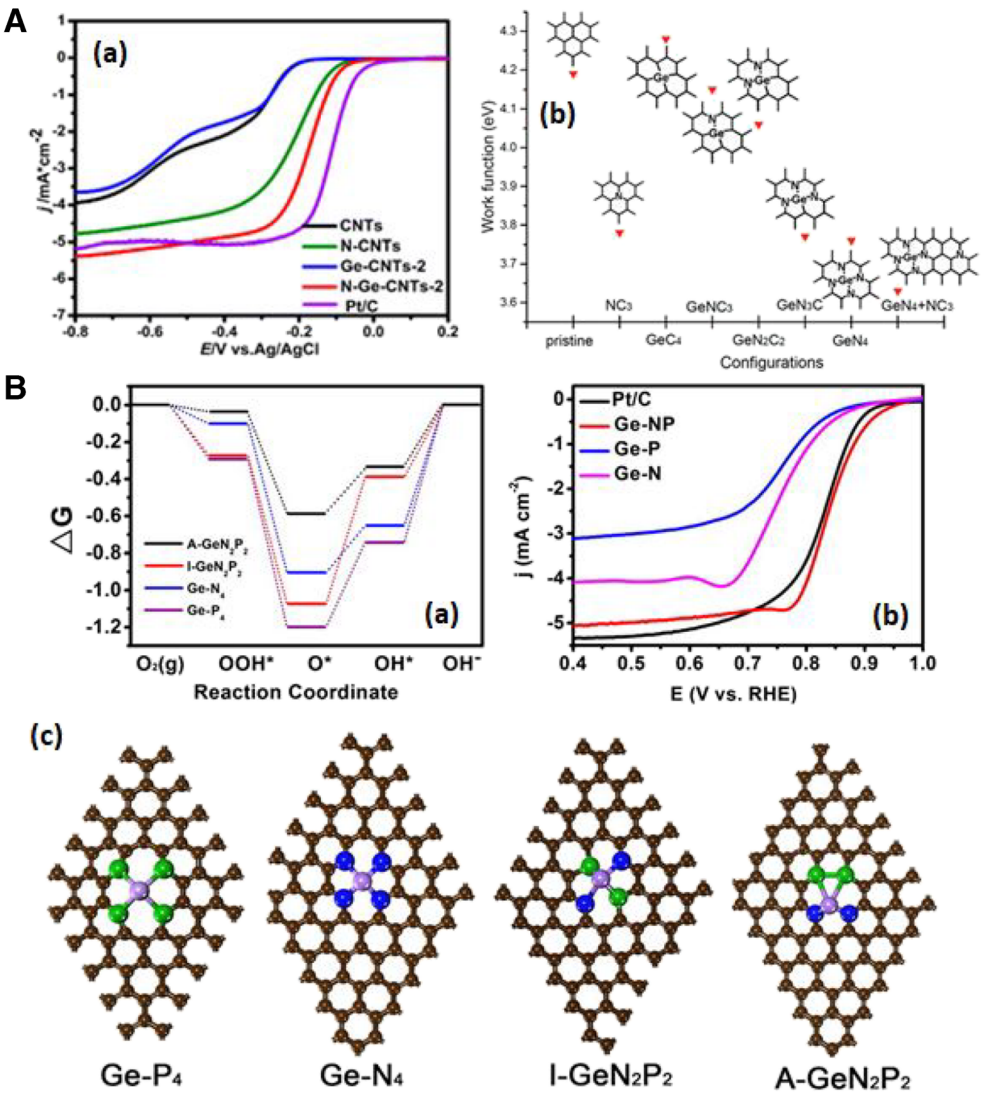

Fig. 6 **a** (a) LSV curves for pure CNTs, doped CNTs, and conventional Pt/C at a rotation rate of 1600 rpm. (b) Calculated work functions for pristine sp^2 carbon and the graphite sheets with different Ge/N mono-co-doping configurations [157] Reprinted with permission from ref. 157 Copyright 2016 American Chemical Society. **b** (a) Schematic free energy diagrams and all relaxed intermediate models for ORR pathway in alkaline condition on Ge-P4, Ge-N_4, I-Ge-N_2P_2, and A-Ge-N_2P_2. (b) ORR performance for Ge-N-P-rGO, Ge-P-rGO, and Ge-N-rGO. (a) LSV polarization curves of the samples. **c** Four different bonding configurations of Ge-P4, Ge-N_4, I-Ge-N_2P_2, and A-Ge-N_2P_2. Dark brown, blue, green, purple, red, and white balls represent C, N, P, and Ge, respectively [158] Reprinted with permission from ref. 158 Copyright 2018 Elsevier

sufficient enough to bring the ORR activity equal to the traditional Pt/C catalysts. Chang et al. [158] investigated a co-doped system of Ge with N- and P-doped carbon and found that the co-doping of P and N effectively reduces the work function of the ORR intermediates and enhances the ORR activity of the Ge system (Ge-NP). They also performed DFT to ascertain the reduced work function and also validate the Ge-NP catalyst by experimental results. Four different bonding configurations of Ge-NP were proposed: (i) GeN_4, (ii) GeP_4, (iii) NP-Ge-NP (A-Ge-N_2P_2), and (iv) NN-Ge-PP (I-Ge-N_2P_2) (Fig. 6c).

From the DFT analysis, authors found a higher electron density around the N atoms and a lower electron density on P and Ge atoms, indicating a bond polarization around the heteroatoms. The lower electron density around the P and Ge atoms is due to the lower electronegativity of P and Ge compared with N. As a result of the synergistic interaction between N and P, Ge species, the determined O_2 adsorption charge on the abovementioned 4 models was found to be 0.90, 0.46, 0.25, and 0.47 e^-. Further, the lower O_2 adsorption on the A–Ge–N_2P_2 configuration is found than on the I–Ge–N_2P_2 configuration and hence A–Ge–N_2P_2 is more favorable for ORR. Moreover, A–Ge–N_2P_2 shows an almost zero band gap compared with all other 3 configurations, further explaining their better ORR activity. Inspired by DFT calculations, authors also synthesized the Ge–N–P–rGO, Ge–P–rGO, and Ge–N–rGO and evaluated their ORR activity in the 0.1-M KOH electrolyte solution. The electrocatalytic analysis indicates that Ge–N–P–rGO catalysts show higher ORR onset and half-wave potentials compared with Ge–P–rGO and Ge–N–rGO catalysts and even higher than the Pt/C catalyst. Moreover, the Ge–N–P–rGO catalyst also performs ORR by a desirable 4-electron transfer process.

Li et al. [159] synthesized the Ge and P co-doped CNTs (Ge–P–CNTs) and evaluated their ORR in the alkaline electrolyte. Ge–P–CNTs were prepared by a solid pyrolysis of the

precursors, where first Ge is doped into the CNTs and then P was subsequently doped. Carboxyethyl germanium sesquioxide and triphenylphosphine were utilized as Ge and P sources. Elemental mapping of Ge-P-CNTs indicates the successful doping of Ge and P atoms into the CNTs. XPS spectra of Ge–P–CNTs show P–Ge bonding at the 133.5 eV, and it was about 8.6 at%, in addition to the P–C and P–O bonding. Further, Ge XPS spectra also show the evidence of C–Ge bonding. This indicates that Ge can also form a bond with P and C to give a Ge–P–CNT structure. Electrochemical ORR analysis indicates that the Ge–CNTs-2 catalysts typically show similar LSV curves with a feature of undesirable 2-electron O_2 reduction reaction. However, after the doping of P (Ge–P–CNTs-2), electrocatalytic activity is enhanced considerably, with a "n" of 3.8. The synergistic ORR activity of Ge-P-CNTs-2 is ascertained by the reduced work function of carbon surface and hence enhances the electron transfer to O_2 to reduce to H_2O.

As a unique approach, Li et al. [160] utilized Ge as the predopant to synthesize S-doped S_{Ge}-CNTs, where Ge is doped firstly and then S is doped to Ge-CNTs to give S_{Ge}-CNTs. The authors found no Ge species in S_{Ge}-CNT_S; only S atoms are found, indicating that Ge atoms promote the S atoms doping into the CNTs. The repeated test indicates that Ge atoms are replaced by S in the subsequent doping. The possible reasons might be that the lower content of Ge might have masked the surface of Ge after S doping. Another possible reason might be that Ge totally disappears after the S doping with Ge acting as the auxiliary dopant for S. This was further confirmed by the increased S content approximately 2–3 times, in S_{Ge}-CNTs when compared with the S-CNT catalyst, strongly suggesting that Ge is the auxiliary dopant for S. The ORR activity investigation of Ge–CNTs, S–CNTs and the different compositions of the S_{Ge}-CNT catalyst by CV and LSV measurements suggest that the S_{Ge}-CNT catalyst showed the highest ORR activity compared with Ge-CNTs and S-CNTs, which the authors described to be due to the higher doping levels of S by the auxiliary role of the Ge dopant. However, the ORR activity is lesser than the Pt/C catalyst. Moreover, keeping in mind the higher boiling point of Ge, the proposed hypothesis needs to be further investigated deeply.

Si is one of the elements from the carbon group element; the electronegativity of Si is much lower than that of carbon (Si = 1.98 and C = 2.55) and hence Si-doped carbons need to be electronically tailored to utilize them effectively for electrocatalytic applications. Recently, Si-doped graphene is found to have high electrocatalytic activity and stability, especially Si-doped di-vacancy graphene [161]. Ramasahayam et al. [162] synthesized P and Si co-doped carbon (SiPDC) by a microwave synthesis method. A suitable composition of a renewable source of tannic (C source), phosphoric acid (P source), and silicon oil (Si source) is subjected to a microwave radiation to obtain the SiPDC catalyst. The XPS atomic composition of SiPDC shows relatively high at% of Si of about 8.80 and P of about 4.20 at% which indicates the successful doping of Si and P into the carbon matrix. In spite of the higher Si and P contents, SiPDC catalysts show only marginal ORR activity, far away from the Pt/C catalysts in the alkaline electrolyte. However, "n" was found to be 3.74 close to a dominant 4 e^- pathway. Ramasahayam et al. [163] synthesized a ternary-doped (phosphorus, nitrogen doped, Si) doped catalyst PNSiDC-3 by utilizing honey as the renewable C source and silicon oil as Si source, and ammonium phosphate as N and P source, by following a similar microwave synthesis protocol, yet the ORR activity of PNSiDC-3 is appreciable but not efficient enough to meet the state-of-the-art Pt/C catalyst. Fu et al. [164] synthesized a series of Si-doped CNTs and investigated their ORR together with the DFT investigations to validate the Si-doped CNTs towards ORR. Si-doped CNTs were synthesized by chemical vapor deposition with xylene as a carbon source and tri-methylphenylsilane as C and Si sources, respectively. ORR activity investigations of Si-doped CNTs were found to be higher than the CNTs. The maximum ORR activity was found with Si-CNTs-2 with a Si atomic percentage of 1.25 at%. However, the ORR curve presents a typical two-step reaction pathway producing higher H_2O_2. This was further confirmed by the estimation of "n" which was found to be 3.06 e^- per O_2 molecule. However, "n" is higher than the baseline CNT catalyst 2.17 e^-, indicating that Si doping has influence on the ORR activity. DFT calculations suggest that the Si doping effectively changes the neighboring carbon atoms surrounding Si which changes the charge from neutral to negative and hence changes the oxygen adsorption energies coupled with a lower energy gap between HUMO and LUMO from 2.75 to 2.21 or 2.01 eV with a single Si and with Si atom doping (Fig. 7a).

Liu et al. [165] synthesized SiN-CNTs and Si-CNTs by thermolysis of 3-aminopropyl-triethoxysilane as a N, C, and Si source, and dimethyl silicone oil as a Si and C source, over the $FeMo/Al_2O_3$ catalyst. XPS analysis shows the confirmation of existence of Si–C and Si–C–O bonds. An electrocatalytic ORR study indicates that Si doping certainly enhances the ORR activity. This was observed in both CV and LSV measurements where SiN-CNTs show a higher ORR onset potentials compared with NCNTs. Further, to ascertain the role of Si towards ORR, the pure CNSs and Si-CNSs were synthesized and it was found that Si-CNSs show higher ORR onset potentials indicating the definite role of Si towards ORR. However, the overall ORR activity of SiN-CNTs is still lesser than that of the Pt/C catalyst. The number of electrons transferred per molecule of O_2 was found to be 2.55 and 3.23 for Si-CNSs and SiN-CNTs, indicating that Si doping enhances the electrotransfer to the O_2 molecule. The performed theoretical energetic calculations suggest that the energy gap between HOMO and LUMO of SiN-CNTs with one and two Si atoms were found to be 2.22 and 1.99 eV compared with

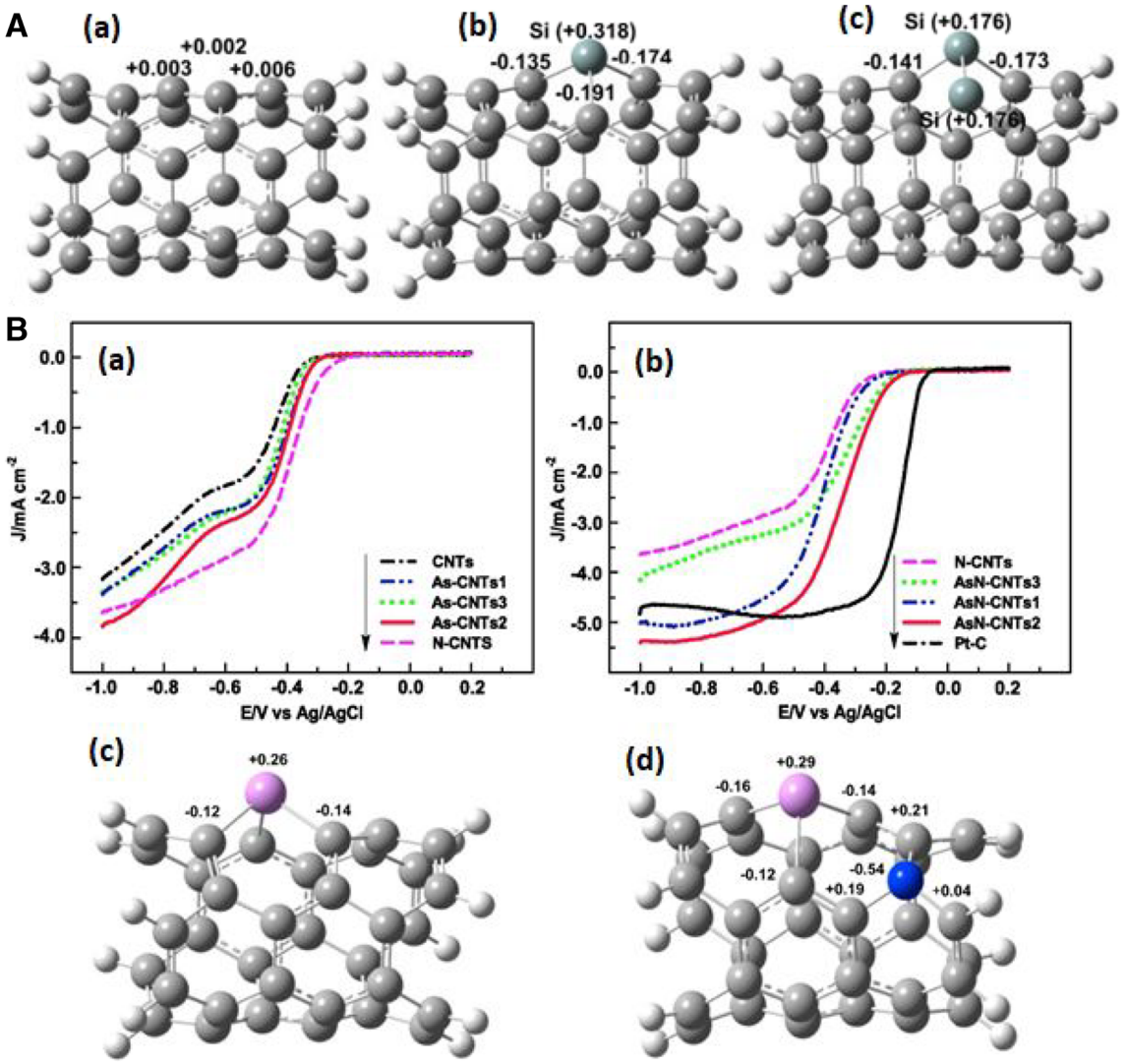

Fig. 7 **a** The net charge distributions of C and Si atoms in pure carbon nanotube (a), Si-doped carbon nanotube with one (b) or two (c) silicon atoms [164] Reprinted with permission from ref. 164 Copyright 2015 Elsevier. **b** Typical LSVs of CNTs, As-CNTs1, As-CNTs2, As-CNTs3, and N-CNTs (b), and N-CNTs, AsN-CNTs1, AsN-CNTs2, AsN-CNTs3, and Pt–C (b) in O_2-saturated 0.1 M KOH aqueous solution at a rotate speed of 600 rpm. (c) The net charge distributions of C, As, and N atoms in As-CNT (d) and AsN-CNT (F) [169] Reprinted with permission from ref. 169 Copyright 2016 American Chemical Society

the non-doped system which was 2.52 eV suggesting that the electron transfer is easier in the Si-doped system. Moreover, Si atoms change the O_2 absorption mode from end-on to side-on absorption and hence help in performing ORR mostly in a direct 4-electron pathway.

Abbas et al. [166] synthesized porous Si-doped carbon catalysts in combination with F doping (SiF-PCM) as an efficient ORR catalyst. Pyrolysis of a mixture of D-glucose, ammonium fluoride, and SiO_2 nanoparticles and successful etching of SiO_2 nanoparticles with HF or NaOH leads to the porous SiF-PCM catalyst. XPS results indicate a clear indication of no Si–F bond formation, and it only shows only semi-ionic and ionic C–F bonds. The estimated atomic percentage of the SiF-PCM catalyst was found to be Si (0.26%), F (0.64%), and N (6.56%). It is observed that the SiF-PCM catalyst also contains a high amount of N and high-resolution spectra of N which shows the existence of pyridinic-N, pyrrolic-N, and graphitic-N. Hence, the overall activity of the SiF-PCM catalyst might come from the synergistic interaction of Si, F, and N. The ORR activity of SiF-PCM is much higher than the undoped, Si-PCM and F-PCM catalysts and is almost comparable with the commercial Pt/C catalyst, with "n" of 4 e^-. The estimated percentage of H_2O_2 is 2.98%, which is almost similar to the Pt/C catalyst (2%), indicating that SiF-PCM is a much effective catalyst compared with the previously established catalysts. The authors claim that enhanced ORR activity is due to the Si doping and existence of semi-ionic and ionic C-F bonds. However, the authors did not consider the ORR activity of N doping effect of SiF-PCM in this study. In addition to the analysis of the catalysts for ORR, the authors

also applied SiF-PCM as the cathode catalyst in microbial fuel cells (MFC). In a single-chambered MFC configuration, SiF-PCM catalysts delivered a power density of 1026 mW m^{-2}, which was higher than 913 mW m^{-2} of a Pt/C catalyst, indicating SiF-PCM as the promising cathode catalyst for MFCs. Esrafili et al. [167] theoretically proposed a possible role of Si as the dopant to the boron nitride nanotubes (Si-BNNTs). Two possible sources of Si doping were found, one near the N site (Si_N) and another one near the B site (Si_B), and found that Si_B-BNNT is energetically favorable and the disociative O_2 reduction reaction proceeds by a 4-electron process more easily than Si_N-BNNTs. However, such systems have not been synthesized experimentally and it is open to the audience to explore the synthetic protocols to synthesize Si_B-BNNT and explore the ORR activity experimentally.

Another metalloid which was proposed for ORR is antimony (Sb). Jeon et al. [168] synthesized metalloid antimony (Sb)–doped graphene platelets (SbGnPs) via a simple mechanochemical ball milling reaction between graphene and metallic Sb. During the ball milling reaction, the carbon edges of graphene react with Sb and form C–Sb bonds. Mechanical ball milling of the graphite and metallic Sb creates an active carbon and Sb species, respectively, and they react together to form C–Sb bonds at the carbon edges. The XPS analysis of SbGNPs exhibits the active Sb^{3+} and Sb^{5+} oxidation states (538.5 and 539.5 eV) of Sb, together with the C–Sb bonds located at 283.6 eV, indicating the successful Sb doping to the graphene platelets. It is also proposed that Sb^{3+} attaches to the zigzag and Sb^{5+} attaches to the armchair edges of SbGnPs. ORR activity evaluation in the 0.1-M KOH electrolyte indicates that SbGnP exhibits enhanced ORR activity when compared with pristine graphite indicating that Sb doping has a certain role in ORR enhancement. Moreover, SbGnPs exhibit excellent durability even after 100,000 cycles indicating the excellent stability of the catalyst. However, when compared with Pt/C catalysts, the SbGnP catalyst shows poor activity. This limitation opens up the way of research to enhance the ORR activity of SbGnP catalysts by other means. DFT calculations suggest that the Sb atoms bonded to two carbon atoms in an armchair and zigzag fashion which are stable and follow a similar trend in the O_2 energy absorption and throughout the ORR pathway. The intermediate state of the ORR process shuttles between Sb^{3+} and Sb^{5+} oxidation states and mostly follows the dissociative ORR pathway to give H_2O as a by-product. To the best of our knowledge, this is the only one article describing the ORR activity of the Sb-doped catalyst; no other reports were found.

Besides its environmental toxicity, arsenic (As) is one of the VA elements and its similar electronic structure with that of N and P could be one of the dopants to carbon. The only study performed on utilizing As, as a dopant, was done by Liu et al. [169]. The authors of this study used As as a dopant in combination with N-doped carbon and applied as a cathode catalyst in alkaline electrolyte. The catalyst was prepared by thermolysis of triphenylarsine, and aniline solutions over the $FeMo/Al_2O_3$ catalyst. As was successfully doped into the CNTs as evidenced by the existence of As–C. C–As–O bonds in the 42.3 and 44.4 eV of As3d spectra. The As-doped CNT catalysts show the typical ORR characteristics (Fig. 7b). Moreover, the ORR activity of As-doped CNTs enhances substantially with N as a secondary dopant (As-NCNTs-2); however, the overall activity is still lesser than that of Pt/C, with a maximum "n" of 3.58 electrons per O_2 molecule. This indicates that the activity of As-doped catalysts needs further improvement, in order to utilize for ORR. DFT theory calculations suggest that the neighboring C atoms around the As and N dopant change their neutral charge to negative. As the electronegativity of As (2.18) is less than C (2.55), charge depolarization occurs and the electroneutrality of the carbon matrix breaks. Moreover, the energy gap between HOMO and LUMO decreases from 2.75 to 2.67 and 2.40 after As doping and As-N doping (Fig. 7c). This would change the electronic structure favoring the O_2 adsorption style and enhancing the electronic transfer kinetics to the adsorbed O_2. Though the As-doped catalyst shows promising ORR activity, other than this study, we could not find any other articles based on As doping. It might be due to the toxic nature of As to the environment; researchers have not focused further in this direction. We have summarized ORR characteristic and fuel cell performances of various heteroatom-doped and metalloid-doped catalysts reported in literatures [170–226] as shown in Tables 1 and 2.

Conclusions and future perspectives

Searching of alternative catalysts for fuel cell cathodic ORR reaction has been the hot topic worldwide last decade. It has been discovered that heteroatom doping dramatically boosts the ORR activity. However, the exact mechanism behind the ORR activity of these doped materials is still a debatable topic. Precise preparative techniques to perform the doping selectively on the edge carbons atoms are still lacking to clearly understand the structure–property relationship of different doped carbons towards ORR. A large number of research reports proposed that the heteroatom-doped catalyst could be promising metal-free catalysts. One should notice that, so far, all the doped carbons' electrochemical ORR activity evaluation was performed in a very fundamental RDE setup. However, in order to realize these metal-free catalysts in a real fuel cell, their power density performance needs to be essentially performed in a more realistic membrane electrode assembly configuration. Only few reports have been really tested in a fuel cell configuration. Hence, the gap between RDE and fuel cell testing needs to be addressed. Moreover, many doped carbon catalysts have been tested in alkaline electrolytes, and only a handful of catalysts have shown a really promising activity in more realistic

Table 1 ORR characteristic of various metalloid and heteroatom doped catalysts in alkaline and acidic electrolytes

Catalyst	Electrolyte	ORR onset potential (V)	$E_{1/2}$	Ref.
Metalloid catalysts				
N–Ge–CNTs-2	0.1 M KOH	− 0.08 vs. Ag/AgCl	NR	[157]
Ge-NP	0.1 M KOH	0.94 vs. RHE	NR	[158]
Ge–P-CNTs-2	0.1 M KOH	− 0.10 vs. Ag/AgCl	NR	[159]
S_{Ge}-CNTs-2	0.1 M KOH	− 0.149 vs. Ag/AgCl	NR	[160]
GeN-CNTs-2	0.1 M KOH	− 0.12 vs. Ag/AgCl	NR	[156]
Si-CNTs-2	0.1 M KOH	− 0.19 vs. Ag/AgCl	NR	[164]
Si-CNTs	0.1 M KOH	− 0.02 vs. Ag/AgCl	NR	[165]
SiF-PCM	0.1 M KOH	0.24 vs. Ag/AgCl	NR	[166]
AsN-CNTs-2	0.1 M KOH	− 0.15 vs. Ag/AgCl	NR	[169]
Si-Fe20/N/C-1_6	0.1 M KOH	1.00 vs. RHE	NR	[170]
Heteroatom-doped catalysts				
C-PCTNB@CNTs	0.1 M $HClO_4$	0.94 vs. RHE	0.85	[171]
Pristine CN_x	0.1 M $HClO_4$	0.76 vs. RHE	0.59	[172]
N-HCS-1000	0.1 M KOH	0.01 vs. Ag/AgCl	0.748	[173]
CNPS-900	0.1 M KOH	− 0.192 vs. Ag/AgCl	NR	[174]
NP-PG-800	0.1 M KOH	− 0.04 vs. Ag/AgCl	− 0.27	[175]
NP-CS	0.1 M KOH	0.02 vs. Ag/AgCl	− 0.11	[112]
N,P-NC-1000	0.1 M KOH	0.01 vs. Ag/AgCl	− 0.13	[176]
CPN-NS	0.1 M KOH	NR vs. Ag/AgCl	0.868	[177]
HP-NPCs-2	0.1 M KOH	− 0.02 vs. Ag/AgCl	− 0.19	[178]
BC	0.1 M KOH	− 0.03 vs. Ag/AgCl	− 0.13	[179]
MPSA/GO-1000	0.1 M KOH	0.01 vs. Ag/AgCl	− 1.6	[180]
NPBC	0.1 M KOH	0.02 vs. Ag/AgCl	− 0.11	[181]
NPMC-950	0.1 M KOH	− 0.02 vs. Ag/AgCl	− 0.17	[182]
NPMC-1000	0.1 M $HClO_4$	0.57 vs. RHE	0.36	[183]
PNDC-10	0.1 M $HClO_4$	0.64 vs. RHE	0.42	[120]
CPAIN-NaCl	0.1 M $HClO_4$	0.60 vs. RHE	0.42	[184]
NrGO	0.1 M $HClO_4$	0.64 vs. RHE	0.45	[115]
ING	0.1 M $HClO_4$	0.59 vs. RHE	0.40	[185]
BCN	0.1 M $HClO_4$	0.58 vs. RHE	0.45	[186]
FN-OMC	0.1 M KOH	NR	− 0.19	[187]
F-MC (5:1)	0.1 M KOH	− 0.16 vs. Ag/AgCl	− 0.28	[188]
NC-D-NH_3	0.1 M KOH	1.00 vs. RHE	NR	[189]
N-PC@G-0.02	0.1 M KOH	1.01 vs. RHE	0.80	[190]
NB-HC	0.1 M KOH	− 0.12 vs. Ag/AgCl	NR	[191]
NHMC-900	0.1 M KOH	1.0 vs. RHE	0.88	[192]
EZIF-C	0.1 M KOH	− 0.030 vs. Ag/AgCl	NR	[193]
N–PC	0.1 M KOH	− 0.02 vs. Ag/AgCl	− 0.198	[80]
N–PC/rGO	0.1 M KOH	− 0.02 vs. Ag/AgCl	− 0.12	[194]
N–PC	0.1 M KOH	− 0.07 (Ag/AgCl)	− 0.161	[195]
N–PC	0.1 M KOH	0.92 vs. RHE	NR	[196]
N–PC/CNT	0.1 M KOH	1.03 vs. RHE	0.88	[197]
N–PC	0.1 M KOH	0.88 vs. RHE	0.81	[198]
N–PC	0.1 M KOH	− 0.08 vs. Ag/AgCl	− 0.15	[199]
N–PC	0.1 M KOH	0.06 vs. Ag/AgCl	− 0.103	[200]
N–PC	0.1 M KOH	0.035 vs Hg/Hgo	NR	[201]
S, N–NC	0.1 M KOH	− 0.005 vs. Ag/AgCl	NR	[202]
N, P, S–PC	0.1 M KOH	− 0.03 vs. Ag/AgCl	− 0.17	[203]
N–PC	0.1 M KOH	0.86 vs. RHE	0.70	[204]
N, P–PC	0.1 M KOH	0.92 vs. RHE	0.8	[205]
N–PC	0.1 M KOH	0.89 vs. RHE	NR	[206]

NR not reported

acid electrolytes, but still far lesser than the Pt/C catalyst. Hence, highly active catalysts are badly needed in acidic electrolytes. A multi-heteroatom doping approach could be a right choice as the synergistic effects by heteroatoms may help to cross over the bridge of Pt/C catalyst activity, in acidic electrolytes. Development of novel membrane electrode assembly architectures is vital for realizing high-performance fuel cells with doped carbon atoms. High loading of the doped carbons in the catalyst layers can significantly increases the mass transfer and contact

Table 2 Fuel cell performance of various heteroatom doped catalysts in alkaline and PEM fuel cells

Catalyst	Fuel cell/condition	Max power density (mW cm^{-2})	Ref.
N-CNTs	Alkaline/H_2-O_2	25.5	[207
N-MWCNTs	Alkaline/H_2-O_2	0.92	[208]
N-graphene	Alkaline/H_2-O_2	2.6	[209]
N-carbon film	Alkaline/H_2-O_2	182	[210]
N-NP graphene	Alkaline/H_2-O_2	27	[211]
N-SWCNH	Alkaline/H_2-O_2	30	[212]
N-HC	Alkaline/H_2-O_2	228	[213]
N-C	Alkaline/H_2-O_2	703	[214]
S-rGO	Alkaline/H_2-O_2	2.83	[215]
F-doped carbon	Alkaline/H_2-O_2	15.56	[106]
N,S-graphene	Alkaline/H_2-O_2	19.8	[216]
NP-OMPC	Alkaline/H_2-O_2	90	[217]
NS-MPC	Alkaline/H_2-O_2	21.7	[218]
N,S-MPC	Alkaline/H_2-O_2	88.2	[219]
N,F-carbon black	Alkaline/H_2-O_2	15	[136]
g-C_3N_4	Alkaline/H_2-O_2	171	[220]
CNT/heteroatom-doped carbon	Alkaline/H_2-O_2	280	[221]
VA-NCNT arrays	PEM/H_2-O_2	230	[222]
P-CNF	PEM/H_2-O_2	330	[223]
UF-C	PEM/H_2-O_2	180	[224]
g-CN-CNF-700	PEM/H_2-O_2	460	[220]
PNCEs	PEM/H_2-O_2	460	[225]
N-CX	PEM/H_2-O_2	360	[226]
NF-GNF	PEM/H_2-O_2	170	[134]

resistances issues in MEAs. As doped carbons are more hydrophilic in nature, applying high loadings can scientifically enhance the overall hydrophilicity of the MEAs and a proper balance between the hydrophilic/hydrophobic ratio is highly required; otherwise, the MEAs will be severely affected with the product water. Hence, a balanced catalyst loading, without compromising the overall activity of the doped carbons, is highly required. All these facts are true also in the case of metalloid-based catalysts. We propose the following future perspectives of metal-free catalysts.

1. Though single heteroatom-doped carbon catalysts have been paid much attention in terms of reaction mechanism, dual-, tri-, and multi-doped heteroatoms' reaction mechanism is still debatable. Hence, more theoretical simulations together with precise doping-controlled experiments are indeed deficiently required for a better understanding of the ORR kinetics.
2. More studies need to be performed to investigate the effect of edge defects and morphology-induced ORR mechanism in various carbon materials such as amorphous carbon, CNTs, and graphene.
3. The exact role of each individual form of heteroatom-doped sites is still not fully understood, such as the debate on the ORR activity of graphitic-N and pyridinic-N and ionic vs semi-ionic vs covalent C–F bonds, as well as five-membered-S and six membered-S doping sites.
4. Investigating the practical usability of heteroatom-doped catalysts especially in practical devices (H_2/O_2 and H_2/Air), in membrane electrode assembly configuration, together with the stability evaluation with standard evaluation protocols, is urgently required, in order to realize the heteroatom-doped catalysts in practical fuel cells.
5. Development of in situ characterization techniques could resolve many questions about the nature of active sites in doped heteroatoms.
6. Combined theoretical simulations and experimental studies are indeed highly required for the better understanding of the reaction mechanisms of doped carbons.
7. Lastly, efforts also need to take interms of synthesizing the catalysts in the bulk level, as required for the industry applications. Hence, scaling the synthetic procedures to a bulk amount, without compromising the dopant concentration and ORR activity, is a challenging issues that needs to be resolved.

Acknowledgments The authors thank Keimyung University, Daegu, Republic of South Korea, for the research support.

Compliance with ethical standards

Conflict of interest The authors declare that they have no conflict of interest.

References

1. Dunn B, Kamath H, Tarascon JM (2011) Electrical energy storage for the grid: a battery of choices. Science 334:928–935
2. Lewis NS, Nocera DG (2006) Powering the planet: chemical challenges in solar energy utilization. Proc Natl Acad Sci U S A 103: 15729–15735
3. Xue B, Qin W, Guangran X, Yunkun N, Keke H, Feng H, Zhi-jian W, Jun Z (2017) Phosphorus and fluorine co-doping induced enhancement of oxygen evolution reaction in bimetallic nitride nanorods arrays: ionic liquid-driven and mechanism clarification. Chem Eur J 23:16862–16870
4. Cheonghee K, Fabio D, Vera B, Xingli W, Tim M, Peter S (2019) Alloy nanocatalysts for the electrochemical oxygen reduction (ORR) and the direct electrochemical carbon dioxide reduction reaction (CO_2RR). Adv Mater 31:1805617–1805636
5. Peera SG, Lee TG, Sahu AK (2019) Pt-rare earth metal alloy/metal oxide catalysts for oxygen reduction and alcohol oxidation reactions: an overview. Sustain Energy Fuels 3:1866–1891
6. Yanli H, Zhan T, Huimin W, Chuanqi F, Yu D (2018) Fe@Pt core-shell nanoparticles as electrocatalyst for oxygen reduction reaction in acidic media. Ionics 24:229–236
7. Jing S, Yan-Ru C, Keke H, Kai L, Qin W (2020) Interfacial electronic structure and electrocatalytic performance modulation in Cu0.81Ni0.19 nanoflowers by heteroatom doping engineering using ionic liquid dopant. Appl Surf Sci 500:144052
8. Yanghua H, Qiang T, Leilei L, Joshua S, Gang W (2019) Metal-nitrogen-carbon catalysts for oxygen reduction in PEM fuel cells: self-template synthesis approach to enhancing catalytic activity and stability. Electrochem Energy Rev 2:231–251
9. Minhua S, Qiaowan C, Jean-Pol D, Regis C (2016) Recent advances in electrocatalysts for oxygen reduction reaction. Chem Rev 116:3594–3657
10. Jing S, Niankun G, Zhiyu S, Keke H, Yaowen L, Feng H, Qin W (2018) A facile strategy to construct amorphous spinel-based electrocatalysts with massive oxygen vacancies using ionic liquid dopant. Adv Energy Mater 8:1800980–1800992
11. Vuri AS, Lukman N, Diah S, Yusuf P, Hsin-Chih H, Sun-Tang C, Kai-Chin W, Chen-Hao W (2019) High oxygen reduction reaction activity on various iron loading of Fe-PANI/C catalyst for PEM fuel cell. Ionics. https://doi.org/10.1007/s11581-019-03240-w
12. Zhang M, Dai L (2012) Carbon nanomaterials as metal-free catalysts in next generation fuel cells. Nano Energy 4:514–517
13. Dingshan Y, Yuhua X, Liming D (2012) Vertically aligned carbon nanotube arrays co-doped with phosphorus and nitrogen as efficient metal-free electrocatalysts for oxygen reduction. J Phys Chem Lett 3:2863–2870
14. Wang S, Iyyamperumal E, Roy A, Xue Y, Yu D, Dai L (2011) Vertically aligned BCN nanotubes as efficient metal-free electrocatalysts for the oxygen reduction reaction: a synergetic effect by co-doping with boron and nitrogen. Angew Chem 123: 11960–11964
15. Chuangang H, Liming D (2016) Carbon-based metal-free catalysts for electrocatalysis beyond the ORR. Angew Chem Int Ed 55:11736–11758
16. Wu J, Pisula W, Müllen K (2007) Graphenes as potential material for electronics. Chem Rev 107:718–747
17. Stoller MD, Park S, Zhu Y, An J, Ruoff RS (2008) Graphene-based ultracapacitors. Nano Lett 8:3498–3502
18. Sahoo NG, PanY LL, Chan SH (2012) Graphene-based materials for energy conversion. Adv Mater 24:4203–4210
19. Wang H, Maiyalagan T, Wang X (2012) Review on recent progress in nitrogen-doped graphene: synthesis, Characterization, and Its Potential Applications. ACS Catal 2:781–794
20. Yang DS, Song MY, Singh KP, Yu JS (2015) The role of iron in the preparation and oxygen reduction reaction activity of nitrogen-doped carbon. Chem Commun 51:2450–2453
21. Yanqiu S, Zhenshuang J, Qiaoqiao Z, Jingqi G (2019) Progress in nonmetal-doped graphene electrocatalysts for the oxygen reduction reaction. ChemSusChem 12:2133–2146
22. Jingjing D, Sheng C, Mietek J, Shi ZQ (2015) Heteroatom-doped graphene-based materials for energy-relevant electrocatalytic processes. ACS Catal 5:5207–5234
23. Dai L, Xue Y, Qu L, Choi HJ, Baek JB (2015) Metal-free catalysts for oxygen reduction reaction. Chem Rev 115:4823–4892
24. Zhenghang Z, Zhenhai X (2016) Design principles for dual-element-doped carbon nanomaterials as efficient bifunctional catalysts for oxygen reduction and evolution reactions. ACS Catal 6: 1553–1558
25. Gengtao F, Yawen T, Jong-Min L (2018) Recent advances in carbon-based bifunctional oxygen electrocatalysts for Zn−air batteries. ChemElectroChem 5:1424–1434
26. Chuangang H, Ying X, Yuqin Z, Liming D (2018) Carbon-based metal-free electrocatalysis for energy conversion, Energy Storage, and Environmental Protection. Electrochem Energy Rev 1:84–112
27. Li Y, Wen H, Yang J, Zhou Y, Cheng X (2019) Boosting oxygen reduction catalysis with N, F, and S tri-doped porous graphene: tertiary N-precursors regulates the constitution of catalytic active sites. Carbon 142:1–12
28. Zhongxin S, Weiwei L, Niancai C, Mohammad NB, Xia L, Qian S, Biwei X, Yulong L, Andrew L, Ruying L, Limin L, Xueliang S (2017) Origin of the high oxygen reduction reaction of nitrogen and sulfur co-doped MOF-derived nanocarbon electrocatalysts. Mater Horiz 4:900–907
29. Zhang L, Xi Z (2011) Mechanisms of oxygen reduction reaction on nitrogen-doped graphene for fuel cells. J Phys Chem C 115:11170–11176
30. Zhao Z, Li M, Zhang L, Xia Z (2015) Design principles for heteroatom-doped carbon nanomaterials as highly efficient catalysts for fuel cells and metal-air batteries. Adv Mater 27:6834–6840
31. Jeon I, Zhang S, Zhang L et al (2013) Edge-selectively sulfurized graphene nanoplatelets as efficient metal-free electrocatalysts for oxygen reduction reaction: the electron spin effect. Adv Mater 25: 6138–6145
32. Dongjiang Y, Lijie Z, Xuecheng Y, Xiangdong Y (2017) Recent progress in oxygen electrocatalysts for zinc–air batteries. Small Methods 1:1700209–1700225
33. Na Y, Xingqun Z, Li L, Jing L, Zidong W (2017) Influence of phosphorus configuration on electronic structure and oxygen reduction reactions of phosphorus-doped graphene. J Phys Chem C 121:19321–19328
34. Tayyaba N, Syed SA, Shah WD, Zidong W (2019) Role of P-doping in antipoisoning: efficient MOF-derived 3D hierarchical architectures for the oxygen reduction reaction. J Phys Chem C 123:16796–16803
35. Sidik RA, Anderson AB, Subramanian NP, Kumaraguru SP, Popov BN (2006) O_2 reduction on graphite and nitrogen-doped graphite: experiment and theory. J Phys Chem B 110:1787–1793
36. Tao G, Zhang L, Chen L, Cui X, Hua Z, Wang M, Wang J, Chen Y, Shi J (2015) N-doped hierarchically macro/mesoporous carbon

with excellent electrocatalytic activity and durability for oxygen reduction reaction. Carbon 86:108–117
37. Ahmed AE, Shaik GP, Nam HK, Joong HL (2019) G-C3N4 templated synthesis of the Fe3C@NSC electrocatalyst enriched with Fe–Nx active sites for efficient oxygen reduction reaction. J Mater Chem A 7:16920–16936
38. Meng Y, Voiry D, Goswami A, Zou X, Huang X, Chhowalla M, Liu Z, Asefa T (2014) N-, O-, and S-tridoped nanoporous carbons as selective catalysts for oxygen reduction and alcohol oxidation reactions. J Am Chem Soc 136:13554–13557
39. Gavrilov N, Pašti IA, Mitri'c M, Travas-Sejdi'c J, Ciri'c-Marjanovi'c G, Mentus SV (2012) Electrocatalysis of oxygen reduction reaction on polyaniline-derived nitrogen-doped carbon nanoparticle surfaces in alkaline media, J. Power Sources 220: 306–316
40. Nam G, Park J, Kim ST, Shin DB, Park N, Kim Y, Lee JS, Cho J (2014) Metal-free ketjenblack incorporated nitrogen-doped carbon sheets derived from gelatin as oxygen reduction catalysts. Nano Lett 14:1870–1876
41. Srinu A, Shaik GP, Akhila KS (2019) Uncovering N, S, F tridoped heteroatoms on porous carbon as a metal-free oxygen reduction reaction catalyst for polymer electrolyte fuel cells. J Electrochem Soc 166:F897–F905
42. Prabhsharan K, Gaurav V, Sekhonc SS (2019) Biomass derived hierarchical porous carbon materials as oxygen reduction reaction electrocatalysts in fuel cells. Prog Mater Sci 102:1–71
43. Zhengping Z, Shaoxuan Y, Hanyu L, Yongxi Z, Xueyan L, Ying Z, Meiling D, Feng W (2019) Sustainable carbonaceous materials derived from biomass as metal-free electrocatalysts. Adv Mater 31:1805718–1805734
44. Srinu A, Bhuvaneswari B, Prabakaran V, Akhila KS (2019) Nitrogen–fluorine dual doped porous carbon derived from silk cotton as efficient oxygen reduction catalyst for polymer electrolyte fuel cells. ACS Appl Energy Mater 2:3253–3263
45. Akula S, Shaik GP, Velayutham P, Balasubramaniam B, Akhila KS (2018) Heteroatom engineering and co–doping of N and P to porous carbon derived from spent coffee grounds as an efficient electrocatalyst for oxygen reduction reactions in alkaline medium. Chemistry Select 3:690–702
46. Shamsunnahar SM, Nagai M (2014) Nitrogen doping of ash-free coal and effect of ash components on properties and oxygen reduction reaction in fuel cell. Fuel 126:134–142
47. Jeon IY, Choi H, Jung S, Seo J, Kim M, Dai L, Baek J (2013) Large-scale production of edge-selectively functionalized graphene nanoplatelets via ball milling and their use as metal-free electrocatalysts for oxygen reduction reaction. J Am Chem Soc 135:1386–1393
48. Hong MK, In-Yup J, In TC, Sung HK, Sun-Hee S, Hu YJ, Myung JJ, Jong-Beom B, Hwan KK (2016) Edge-selectively antimony-doped graphene nanoplatelets as an outstanding counter electrode with an unusual electrochemical stability for dye-sensitized solar cells employing cobalt electrolytes. J Mater Chem A 4:9029–9037
49. Gong K, Du F, Xia Z, Durstock M, Dai L (2009) Nitrogen-doped carbon nanotube arrays with high electrocatalytic activity for oxygen reduction. Science 323:760–764
50. Qu L, Liu Y, Baek JB, Dai L (2010) Nitrogen-doped graphene as efficient metal-free electrocatalyst for oxygen reduction in fuel cells. ACS Nano 4:1321–1326
51. Hao J, Jinxing G, Xusheng Z, Min L, Xiaoqing Q, Liangbing W, Wenzhang L, Zhongfang C, Xiaobo J, Jie L (2019) Defect-rich and ultrathin N doped carbon nanosheets as advanced trifunctional metal-free electrocatalysts for the ORR, OER and HER. Energy Environ Sci 12:322–333
52. Xiangyu L, Dan W, Liping G, Lihui X, Haiyan Z, Lilai L, Jinqiu Z, Maozhong A, Peixia Y (2018) Enriched graphitic N in nitrogen-doped graphene as a superior metal-free electrocatalyst for the oxygen reduction reaction. New J Chem 42:19665–19670
53. Wu X, Keqiu C, Zhipeng L, Yuanming Z, Hui M (2019) Nitrogen doped graphitic carbon from biomass as non-noble metal catalyst for oxygen reduction reaction. Mater Today Energ 13:100–108
54. Lijun Y, Jianglan S, Lei D, Yuyan S, Jun L, Liming D, Zheng H (2019) Carbon-based metal-free ORR electrocatalysts for fuel cells: past, present, and future. Adv Mater 31:1804799–1804819
55. Junghoon O, Sunghee P, Dawoon J, Yunseok S, Donggyu L, Sungjin P (2019) Metal-free N-doped carbon blacks as excellent electrocatalysts for oxygen reduction reactions. Carbon 145:481–487
56. Haijing D, Qian L, Jingjun L, Feng W (2017) Active sites for oxygen reduction reaction on nitrogen-doped carbon nanotubes derived from polyaniline. Carbon 112:219–229
57. Ziyin L, Gordon HW, Yan L, Meilin L, Ching-ping W (2013) Simple preparation of nanoporous few-layer nitrogen-doped graphene for use as an efficient electrocatalyst for oxygen reduction and oxygen evolution reactions. Carbon 53:30–136
58. Dingshan Y, Qiang Z, Liming D (2010) Highly efficient metal-free growth of nitrogen-doped single-walled carbon nanotubes on plasma-etched substrates for oxygen reduction. J Am Chem Soc 132:15127–15129
59. Matter PH, Zhang L, Ozkan US (2006) The role of nanostructure in nitrogen-containing carbon catalysts for the oxygen reduction reaction. J Catal 239:83–96
60. Jing L, Ping S, Weilin X (2017) Structure-activity relationship of doped-nitrogen (N)-based metal-free active sites on carbon for oxygen reduction reaction. Carbon 115:763–772
61. Zheng H, Zuowei L, Wenji Y, Haihui Z, Chaopeng F, Yi G, Liang C, Yafei K (2017) Different types of nitrogen species in nitrogen-doped carbon material: the formation mechanism and catalytic role on oxygen reduction reaction. Electrochim Acta 245:957–966
62. Wei W, Haiwei L, Khaled P, Xiaodong Z, Xinliang F, Klaus M (2014) Nitrogen-doped carbon nanosheets with size-defined mesopores as highly efficient metal-free catalyst for the oxygen reduction reaction. Angew Chem 126:1596–1600
63. Tuci G, Zafferoni C, Rossin A, Milella A, Luconi L, Innocenti M, Truong P, Duong-Viet C, Pham-Huu C, Giambastiani G (2014) Chemically functionalized carbon nanotubes with pyridine groups as easily tunable N-decorated nanomaterials for the oxygen reduction reaction in alkaline medium. Chem Mater 26:3460–3470
64. Ma F, Wang J, Wang FB, Xia XH (2015) The room temperature electrochemical synthesis of N-doped graphene and its electrocatalytic activity for oxygen reduction. Chem Commun 51:1198–1201
65. Gao S, Liu H, Geng K, Wei X (2015) Honeysuckles-derived porous nitrogen, sulfur, dual-doped carbon as high-performance metal-free oxygen electroreduction catalyst. Nano Energy 12:785–793
66. Wenjie L, Qianxun R, Shixiang Z, Song Y, Jie H, Chao Y (2019) Controllable synthesis of nitrogen-doped carbon nanotubes derived from halloysite-templated polyaniline towards nonprecious ORR catalysts. Appl Surf Sci 469:269–275
67. James AB, Alessandro I, Carlota D, Serban NS, Md. Khairul H, Joana MV, Tatiana SP, Paula EC (2019) Electrocatalysis of N-doped carbons in the oxygen reduction reaction as a function of pH: N-sites and scaffold effects. Carbon 148:224–230
68. Marco F, Lara F, Gianluca F, Luciano C, Cristiana DV, Christian D, Francesco S, Armando G, Stefano A, Gaetano G (2015) Single and multiple doping in graphene quantum dots: unraveling the origin of selectivity in the oxygen reduction reaction. ACS Catal 5:129–144
69. Xiaoli W, Qin X, Bin H, Jing N, Wei Y, Huanbao F, Changguo C (2018) A promising graphitic N-dominated porous carbon catalyst

derived from lotus leaves for oxygen reduction reaction. Ionics 24: 3601–3609
70. Liu Y, Xiaofei Z, Wenchuan W, Dapeng C (2018) Recent progress in MOF-derived, heteroatom-doped porous carbons as highly efficient electrocatalysts for oxygen reduction reaction in fuel cells. Adv Funct Mater 28:1704537–1704558
71. Yu-Zhen C, Rui Z, Long J, Hai-Long J (2018) Metal–organic framework-derived porous materials for catalysis. Coord Chem Rev 362:1–23
72. Shaofang F, Chengzhou Z, Junhua S, Dan D, Yuehe L (2017) Metal-organic framework-derived non-precious metal nanocatalysts for oxygen reduction reaction. Adv Energy Mater 7:1700363–1700382
73. Carlos PC, Carlos OA, José BP, Conchi OA, Rumoria P, Turnes PG (2015) A rapid microwave-assisted synthesis of a sodium–cadmium metal–organic framework having improved performance as a CO2 adsorbent for CCS. Dalton Trans 44:9955–9963
74. AliMorsali M (2015) Sonochemical synthesis of a nano-structured zinc(II) amidic pillar metal–organic framework. Ultrason Sonochem 27:416–422
75. Alireza AT, Vahid S, Ali M, Giuseppe B, Hadi HR (2015) Ultrasound-assisted synthesis of metal–organic framework nanorods of Zn-HKUST-1 and their templating effects for facile fabrication of zinc oxide nanorods via solid-state transformation, inorganic Chem. Commun. 59:41–45
76. Dey C, Kundu T, Biswal BP, Mallick A, Banerjee R (2014) Crystalline metal-organic frameworks (MOFs): synthesis, structure and function. Acta Cryst B70:3–10
77. Yuchen P, Zhiyuan Q, Xinle L, Raghu VMG, Tian WG, Chaoxian X, Tianyu W, Wenyu H (2017) Morphology inherence from hollow MOFs to hollow carbon polyhedrons in preparing carbon-based electrocatalysts. J Mater Chem A 5:186–6192
78. Tan A-d, Yi-fang W, Zhi-yong F, Panagiotis T, Liang Z-x (2017) Highly effective oxygen reduction reaction electrocatalysis: nitrogen-doped hierarchically mesoporous carbon derived from interpenetrated nonporous metal-organic frameworks. Appl Catal B 218:260–266
79. Linjie Z, Zixue S, Feilong J, Lingling Y, Jinjie Q, Youfu Z, Wenmu L, Maochun H (2014) Highly graphitized nitrogen-doped porous carbon nanopolyhedra derived from ZIF-8 nanocrystals as efficient electrocatalysts for oxygen reduction reactions. Nanoscale 6:6590–6602
80. Wu M, Wang K, Yi M, Tong Y, Wang Y, Song S (2017) A facile activation strategy for an MOF-derived metal-free oxygen reduction reaction catalyst: direct access to optimized pore structure and nitrogen species. ACS Catal 7:6082–6088
81. Qian R, Hui W, Xue-Feng L, Ye-Xiang T, Gao-Ren L (2018) Recent progress on MOF-derived heteroatom-doped carbon-based electrocatalysts for oxygen reduction reaction. Adv Sci 5: 1700515–1700536
82. Lei D, Lixin X, Gaixia Z, Shuhui S (2020) Metal-organic framework derived carbon materials for electrocatalytic oxygen reactions: recent progress and future perspectives. Carbon 156:77–92
83. Zhongxin S, Niancai C, Andrew L, Xueliang S (2016) Recent progress on MOF-derived nanomaterials as advanced electrocatalysts in fuel cells. Catalysts 6:116–135
84. Sumin S, Dongwook L, Daehyeon N, Jieun K, Sang ES, Sung-Hyeon B (2019) N, S-doped nanocarbon derived from ZIF-8 as a highly efficient and durable electro-catalyst for oxygen reduction reaction. J Solid State Chem 274:237–242
85. Wendan X, Qixing Z, Fengxiang L, Brim SO (2019) Zeolitic imidazolate framework-8 (ZIF-8) as robust catalyst for oxygen reduction reaction in microbial fuel cells. J Power Sources 423: 9–17
86. Peike C, Yanming L, Xie Q, Jujiao Z, Shuo C, Hongtao Y (2019) Nitrogen-doped hierarchically porous carbon nanopolyhedras derived from core-shell ZIF-8@ZIF-8 single crystals for enhanced oxygen reduction reaction. Catal Today 327:366–373
87. Shasha L, Zhongqing J, Xunwen X, Weiheng C, Xiaoning T, Xiaogang H, Zhong-Jie J (2019) MOF-derived Co nanoparticles embedded in N, S-codoped carbon layer/MWCNTs for efficient oxygen reduction in alkaline media. Ionics 25:785–796
88. Zhen-Huan S, Hong-Li G, Wen-Jing B, Feng-Bin W, Xing-Hua X (2012) Synthesis of boron doped graphene for oxygen reduction reaction in fuel cells. J Mater Chem 22:390–395
89. Xiangjie B, Liping G (2013) Ordered mesoporous boron-doped carbons as metal-free electrocatalysts for the oxygen reduction reaction in alkaline solution. Phys Chem Chem Phys 15:2459–2465
90. Yang LJ, Jiang SJ, Zhao Y et al (2011) Boron-doped carbon nanotubes as metal-free electrocatalysts for the oxygen reduction reaction. Angew Chem Int Ed 50:7132–7135
91. Liu ZW, Peng F, Wang HJ, Yu H, Zheng WX, Yang J (2011) Phosphorus-doped graphite layers with high electrocatalytic activity for the O_2 reduction in an alkaline medium. Angew Chem Int Ed 50:3257–3261
92. Ziwu L, Feng P, Hongjuan W, Hao Y, Tan J, Lili Z (2011) Novel phosphorus-doped multiwalled nanotubes with high electrocatalytic activity for O_2 reduction in alkaline medium. Catal Commun 16:35–38
93. Dae-SooY DB, Min YS, Jong-Sung Y (2014) Carbon highly efficient metal-free phosphorus-doped platelet ordered mesoporous carbon for electrocatalytic oxygen reduction. Carbon 67:736–743
94. Jiao W, Chao J, Zhenrong Y, Jinhua T, Ruizhi Y (2015) Synthesis of phosphorus-doped carbon hollow spheres as efficient metal-free electrocatalysts for oxygen reduction. Carbon 82:562–571
95. Meng-qing G, Jia-qi H, Xiang-yi K, Hong-jie P, Han S, Fang-yuan Q, Lin Z, Wan-cheng Z, Qiang Z (2016) Hydrothermal synthesis of porous phosphorus-doped carbon nanotubes and their use in the oxygen reduction reaction and lithium-sulfur batteries. New Carbon Mater 31:352–362
96. Wu J, Yang R, Yan W (2019) Phosphorus-doped hierarchical porous carbon as efficient metal-free electrocatalysts for oxygen reduction reaction. Int J Hydrog Energy 44:12941–12951
97. Lipeng Z, Jianbing N, Mingtao L, Zhenhai X (2014) Catalytic mechanisms of sulfur-doped graphene as efficient oxygen reduction reaction catalysts for fuel cells. J Phys Chem C 118:3545–3553
98. Wanqing L, Duanguang Y, Hongbiao C, Yong G, Huaming L (2015) Sulfur-doped carbon nanotubes as catalysts for the oxygen reduction reaction in alkaline medium. Electrochim Acta 165:191–197
99. In-Yup J, Hyun-Jung C, Min C, Jeong-Min S, Sun-Min J, Min-Jung K, Sheng Z, Lipeng Z, Zhenhai X, Liming D, Noejung P, Jong-Beom B (2013) Facile, scalable synthesis of edge-halogenated graphene nanoplatelets as efficient metal-free eletrocatalysts for oxygen reduction reaction. Sci Rep 3:1810–1817
100. Yunfeng Z, Jilin H, Zhipeng L, Xiang Y, Dongrong Z, Xiaoxue Z, Fangyan X, Weihong Z, Jian C, Hui M (2015) Iodine/nitrogen co-doped graphene as metal free catalyst for oxygen reduction reaction. Carbon 95:930–939
101. Zhen Y, Huagui N, Zhi Y, Xuemei Z, Zheng L, Shaoming H (2012) Catalyst-free synthesis of iodine-doped graphenevia a facile thermal annealing process and its use for electrocatalytic oxygen reduction in an alkaline medium. Chem Commun 48:1027–1029
102. In-Yup J, Changmin K, Guntae K, Jong-Beom B (2015) Mechanochemically driven iodination of activated charcoal for metal-free electrocatalyst for fuel cells and hybrid Li-air cells. Carbon 93:465–472
103. Takahiro I, Yuta W, Satoshi C, Sou K, Hoonseung L, Ai S, Oi LL, Gasidit P (2016) Effects of halogen doping on nanocarbon

catalysts synthesized by a solution plasma process for the oxygen reduction reaction. Phys Chem Chem Phys 18:21843–21851
104. Xiujuan S, Yuwei Z, Ping S, Jing P, Lin Z, Weilin X, Wei X (2013) Fluorine-doped carbon blacks: highly efficient metal-free electrocatalysts for oxygen reduction reaction. ACS Catal 3: 1726–1729
105. Xiujuan S, Ping S, Tao C, Jing L, Weilin X (2013) Fluorine-doped BP 2000: highly efficient metal-free electrocatalysts for acidic oxygen reduction reaction with superlow H_2O_2 yield. Chem Commun 49:10296–10298
106. Hui-Juan Z, Sunwu Y, Jing G, Zi-Feng M, Junhe Y (2019) Oxygen reduction reaction with efficient, metal-free nitrogen, fluoride-codoped carbon electrocatalysts derived from melamine hydrogen fluoride salt. J Colloid Interface Sci 535:436–443
107. Lulun C, Xiaolong X, Wenxiu Y, Jianbo J (2019) Recent advances in carbon-based electrocatalysts for oxygen reduction reaction. Chin Chem Lett. https://doi.org/10.1016/j.cclet.2019.08.008
108. Taizhong H, Shun M, Ming Q, Ou M, Chris Y, Junhong C (2016) Nitrogen-boron dipolar-doped nanocarbon as a high-efficiency electrocatalyst for oxygen reduction reaction. Electrochim Acta 222:481–487
109. Rachel JK, Wisit H, Jessica C, Michael JI, Robert AWD (2019) Well-defined boron/nitrogen-doped polycyclic aromatic hydrocarbons are active electrocatalysts for the oxygen reduction reaction. Chem Mater 316:1891–1898
110. Yao Z, Yan J, Lei G, Mietek J, Shi ZQ (2013) Two-step boron and nitrogen doping in graphene for enhanced synergistic catalysis. Angew Chem Int Ed 52:3110–3116
111. Shuangyin W, Lipeng Z, Zhenhai X, Ajit R, Dong WC, Jong-Beom B, Liming D (2012) BCN graphene as efficient metal-free electrocatalyst for the oxygen reduction reaction. Angew Chem 124:4285–4288
112. Tao S, Jun W, Chuntian Q, Xiang L, Bingbing T, Wei C, Chenliang S (2018) B, N Codoped and defect-rich nanocarbon material as a metal-free bifunctional electrocatalyst for oxygen reduction and evolution reactions. Adv Sci 5:1800036–1800045
113. Jiemin W, Jian H, Dan L, Si Q, David P, Yinwei L, Ying C, Weiwei L (2017) Porous boron carbon nitride nanosheets as efficient metal-free catalysts for the oxygen reduction reaction in both alkaline and acidic solutions. ACS Energy Lett 2:306–312
114. Wei W, Pengde W, Yumao K, Jiao Z, Pengyu T, Ziqiang L (2019) Flame synthesis of nitrogen, boron co-doped carbon as efficient electrocatalyst for oxygen reduction reaction. Int J Hydrog Energy 44:4771–4779
115. Jie Y, Congliang W, Wenjing Y, Yuhua S, Anjian X (2019) B, N co-doped three-dimensional carbon aerogels with excellent electrochemical performance for the oxygen reduction reaction. Chem Eur J 25:2877–2883
116. Yunjie Z, Yue S, Huibo W, Cheng Z, Jin G, Dan W, Hui H, Yang L, Zhenhui K (2018) A nitrogen and boron co-doped metal-free carbon electrocatalyst for an efficient oxygen reduction reaction. Inorg Chem Front 5:2985–2991
117. Chang HC, Sung HP, Seong IW (2012) Phosphorus–nitrogen dual doped carbon as an effective catalyst for oxygen reduction reaction in acidic media: effects of the amount of P-doping on the physical and electrochemical properties of carbon. J Mater Chem 22: 12107–12115
118. Ya-Nan S, Ming-Li Z, Li Z, Zhu-Yin S, Zhen-Yu S, Bao-Hang H (2019) A N, P dual-doped carbon with high porosity as an advanced metal-free oxygen reduction catalyst. Adv Mater Interfaces 6:1900592–1900601
119. Rong L, Huinan L, Jilan L, Jing H, Jimin Z, Hongying Z, Xinglong G (2018) Nitrogen and phosphorus dual-doped porous carbon nanosheets for efficient oxygen reduction in both alkaline and acidic media. ChemCatChem 10:4038–4046
120. Denis PA, Huelmo CP, Iribarne F (2014) Theoretical characterization of sulfur and nitrogen dual-doped graphene. Comput Theor Chem 1049:13–19
121. Ai W, Luo Z, Jiang J, Zhu J, Du Z, Fan Z, Xie L, Zhang H, Huang W, Yu T (2014) Nitrogen and sulfur codoped graphene: multifunctional electrode materials for high-performance Li-ion batteries and oxygen reduction reaction. Adv Mater 26:6186–6192
122. Konggang Q, Yao Z, Sheng D, Shi ZQ (2016) Graphene oxide-polydopamine derived N, S-codoped carbon nanosheets as superior bifunctional electrocatalysts for oxygen reduction and evolution. Nano Energy 19:373–381
123. Arunchander A, Peera SG, Subhendu KP, Chellammal S, Sahu AK (2017) Simultaneous co-doping of N and S by a facile in-situ polymerization of 6-N,N-dibutylamine-1,3,5-triazine-2,4-dithiol on graphene framework: an efficient and durable oxygen reduction catalyst in alkaline medium. Carbon 118:531–544
124. Hui W, Liang S, Jiaheng L, Dan L, Deyu Q, Zhizhong X, Xiaodi D, Peng Y, Xiaosong H, Junsheng L, Haolin T (2016) Nitrogen and sulfur co-doped carbon with three-dimensional ordered macroporosity: an efficient metal-free oxygen reduction catalyst derived from ionic liquid, J. Power Sources 323:90–96
125. Yiyi S, Jinfan C, Chengxu Z, Zhouguang L, Meng N, Patrick HL, Sit M, Leung KH (2018) Nitrogen-doped graphene derived from ionic liquid as metal-free catalyst for oxygen reduction reaction and its mechanisms. Appl Energy 225:513–521
126. Cuie Z, Jinxiang L, Yan C, Jianyu C (2019) Nitrogen and sulfur dual-doped graphene as an efficient metal-free electrocatalyst for the oxygen reduction reaction in microbial fuel cells. New J Chem 43:9389–9395
127. Yunfeng Z, Jilin H, Zhipeng L, Xiang Y, Dongrong Z, Xiaoxue Z, Fangyan X, Weihong Z, Jian C, Hui M (2015) Nitrogen and sulfur dual-doped graphene as an efficient metal-free electrocatalyst for the oxygen reduction reaction in microbial fuel cells. Carbon 95: 930–939
128. Wen-Ju L, Ya-Qiong W, Jia-Wei W, Di-Chang Z, Jing-Bo T, Tong-Bu L (2019) Nitrogen- and iodine-doped microporous carbon derived from a hydrogen-bonded organic framework: an efficient metal-free electrocatalyst for the oxygen reduction reaction. J Mater Chem A 7:9587–9592
129. Marinoiu A, Raceanu M, Carcadea E, Varlam M, Stefanescu I (2019) Iodinated carbon materials for oxygen reduction reaction in proton exchange membrane fuel cell. Scalable synthesis and electrochemical performances. Arab J Chem 12:868–880
130. Adrian M, Mirce R, Elena C, Mihai V (2018) Iodine-doped graphene – catalyst layer in PEM fuel cells. Appl Surf Sci 456: 238–245
131. Jong YB, In-Yup J, Jong-Beom B (2014) Edge-iodine/sulfonic acid-functionalized graphene nanoplatelets as efficient electrocatalysts for oxygen reduction reaction. J Mater Chem A 2:8690–8695
132. Kiran PS, Min YS, Jong-Sung Y (2014) Iodine-treated heteroatom-doped carbon: conductivity driven electrocatalytic activity. J Mater Chem A 2:18115–18124
133. Xiujuan S, Ping S, Yuwei Z, Changpeng L, Weilin X, Wei X (2013) A class of high performance metal-free oxygen reduction electrocatalysts based on cheap carbon blacks. Sci Rep 3:2505–2510
134. Peera SG, Sahu AK, Arunchander A, Bhat SD, Karthikeyan J, Murugan P (2015) Nitrogen and fluorine co-doped graphite nanofibers as high durable oxygen reduction catalyst in acidic media for polymer electrolyte fuel cells. Carbon 93:130–142
135. Srinu A, Parthiban V, Peera SG, Singh BP, Dhakate SR, Sahu AK (2017) Simultaneous co-doping of nitrogen and fluorine into MWCNTs: an in-situ conversion to graphene like sheets and its electro-catalytic activity toward oxygen reduction reaction. J Electrochem Soc 164:F568–F576

136. Kevin NW, Svitlana P, Tim SO, Arrelaine AD, Kevin ON, Steven TC, Huyen ND, Thomas G, Ryan O'H (2012) Effect of halide-modified model carbon supports on catalyst stability. ACS Appl Mater Interfaces 4:6728–6734
137. Peera SG, Arunchander A, Sahu AK (2016) Platinum nanoparticles supported on nitrogen and fluorine co-doped graphite nanofibers as an excellent and durable oxygen reduction catalyst for polymer electrolyte fuel cells. Carbon 107:667–679
138. Peera SG, Arunchander A, Sahu AK (2016) Cumulative effect of transition metals on nitrogen and fluorine co-doped graphite nanofibers: an efficient and highly durable non-precious metal catalyst for the oxygen reduction reaction. Nanoscale 8:14650–14664
139. Shaofang F, Chengzhou Z, Junhua S, Mark HE, Biwei X, Dan D, Yuehe L (2017) Nitrogen and fluorine-codoped carbon nanowire aerogels as metal-free electrocatalysts for oxygen reduction reaction. Chem Eur J 23:10460–10464
140. Xiaochang Q, Shijun L, Guanghua W, Ruiping Z, Huiyu S, Xiuhua L (2016) Simultaneous doping of nitrogen and fluorine into reduced graphene oxide: a highly active metal-free electrocatalyst for oxygen reduction. Carbon 99:272–279
141. Tianle G, Ruoyu Q, Xundao L, Hong L, Yongming Z (2019) N, F-codoped microporous carbon nanofibers as efficient metal-free electrocatalysts for ORR. Nano Micro Lett 11:9–20
142. Xi ST, Qi Z, Yan L, Xiaoling L, Delong M, Heng-guo W (2019) N, P, S tri-doped hollow carbon nanosphere as a high-efficient bifunctional oxygen electrocatalyst for rechargeable Zn-air batteries. Appl Surf Sci 490:47–55
143. Yongxi Z, Zhengping Z, Meiling D, Feng W (2019) Enhancement mechanism of sulfur dopants on the catalytic activity of N and P co-doped three-dimensional hierarchically porous carbon as a metal-free oxygen reduction electrocatalyst. Catal Sci Technol. https://doi.org/10.1039/C9CY01387C
144. Fan M, Yang H, Fanshu Y, Qingli H, Jiazhi Y, Dongping S (2017) Effects of multiple heteroatom species and topographic defects on electrocatalytic and capacitive performances of graphene. J Power Sources 366:143–150
145. Ya-Nan Z, Chang-Yan C, Wen-Jie J, Shu-Liang Y, Jin-Song H, Wei-Guo S, Li-Jun W (2016) Nitrogen, phosphorus and sulfur co-doped ultrathin carbon nanosheets as a metal-free catalyst for selective oxidation of aromatic alkanes and the oxygen reduction reaction. J Mater Chem A 4:18470–18477
146. Haoqing R, Tianrong Z, Yuan S, Yonghong W, Xien L, Hongni T (2019) ZIF-8 derived nitrogen, phosphorus and sulfur tri-doped mesoporous carbon for boosting electrocatalysis to oxygen reduction in universal pH rang. Electrochim Acta 318:783–793
147. Jintao Z, Liming D (2016) Nitrogen, phosphorus, and fluorine tri-doped graphene as a multifunctional catalyst for self-powered electrochemical water splitting. Angew Chem Int Ed 55:13296–11330
148. Lei W, Yueqing W, Mingguang W, Zengxi W, Chunyu C, Minglei M, Jintao Z, Xiaopeng H, Quanhui L, Ma J (2018) Nitrogen, fluorine, and boron ternary doped carbon fibers as cathode electrocatalysts for zinc–air batteries. Small 14:1800737–1800744
149. Sen L, Guozhu L, Yuying G, Zhourong X, Junfeng Z, Qingfa W, Xiangwen Z, Li W (2017) Doping carbon nanotubes with N, S, and B for electrocatalytic oxygen reduction: a systematic investigation on single, double, and triple doped modes. Catal Sci Technol 7:4007–4016
150. Chuyen VP, Benjamin B, Thomas B, Steven H, Simon T (2018) Doped, defect-enriched carbon nanotubes as an efficient oxygen reduction catalyst for anion exchange membrane fuel cells. Adv Mater Interfaces 5:1800184–1800193
151. Kathrin P, Adaeze MS, Cristina IB, Maria-Magdalena T (2019) The influence of heteroatom dopants nitrogen, boron, sulfur, and phosphorus on carbon electrocatalysts for the oxygen reduction reaction. ChemPlusChem 84:457–464
152. Minjoo LL, Leitz CW, Cheng Z, Pitera AJ, Langdo T, Currie MT, Taraschi G, Fitzgerald EA (2001) Strained Ge channel p-type metal–oxide–semiconductor field-effect transistors grown on $Si_{1-x}Ge_x$/Si virtual substrates. Appl Phys Lett 79:3344–3346
153. Chang HK, Hyung SI, Yong JC, Chan SJ, Dong MJ, Yoon M, Han SK, Seung HB, Young RL, Chi-Woo L, Jeunghee P, Min SS, Won-Il C (2012) High-yield gas-phase laser photolysis synthesis of germanium nanocrystals for high-performance photodetectors and lithium ion batteries. J Phys Chem C 116:26190–26196
154. Dunwei W, Ying-Lan C, Qian W, Jien C, Damon BF, Roy GG, Hongjie D (2004) Surface chemistry and electrical properties of germanium nanowires. J Chem Soc Chem 126:11602–11611
155. Takagi S (2003) Re-examination of subband structure engineering in ultra-short channel MOSFETs under ballistic carrier transport. VLSI Symp Technol Dig 14:115–116
156. Fang W, Ziwu L, Meng L, Quan-De W (2016) Germanium-doped and germanium/nitrogencodoped carbon nanotubes with highly enhanced activity for oxygen reduction in alkaline medium. RSC Adv 6:72676–72680
157. Xilin S, Qianqian L, Na M, Jin S, Dengwei J, Chengmeng C, Lijun Y, Dongjiang Y (2016) Creation of $Ge{-}N_x{-}C_y$ configures in carbon nanotubes: origin of enhanced electrocatalytic performance for oxygen reduction reaction. ACS Appl Mater Interfaces 8:10383–10391
158. Guojing C, Jun R, Xilin S, Kewei W, Sridhar K, Dongjiang Y (2018) How heteroatoms (Ge, N, P) improve the electrocatalytic performance of graphene: theory and experiment. Sci Bull 63:155–158
159. Qianqian L, Fang Y, Chunyun Y, Jianjie Z, Jin S, Yijun W, Jun R, Xilin S (2016) Germanium and phosphorus co-doped carbon nanotubes with high electrocatalytic activity for oxygen reduction reaction. RSC Adv 6:33205–33211
160. Kangming L, Xiaoyang C, Yumeng H, Juan W, Tenglong Z, Zhigang W, Yang Y, Chenguang L, Sibudjing K, Qin Z (2018) Understanding the effect of germanium as an efficient auxiliary pre-dopant in carbon nanotubes on enhancing oxygen reduction reaction. Energy Technol 6:2387–2393
161. Xiaowan B, Erjun Z, Kai L, Ying W, Menggai J, Feng H, Xiaoxu S, He S, Zhijian W (2016) Theoretical investigation on the reaction pathways for oxygen reduction reaction on silicon doped graphene as potential metal-free catalyst. J Electrochem Soc 163:F1496–F1502
162. Sunil KR, Udaya BN, Venugopal B, UShaikh A, Tito V (2014) Microwave assisted synthesis and characterization of silicon and phosphorous co-doped carbon as an electrocatalyst for oxygen reduction reaction. RSC Adv 4:6306–6313
163. Sunil KR, Tito V (2016) Honey-based P, N and Si tri-doped graphitic carbon electrocatalysts for oxygen reduction reaction in alkaline conditions. Chem Select 1:3527–3534
164. Xin F, Quan-DW ZL, Feng P (2015) Si-doped carbon nanotubes as efficient metal-free electrocatalysts for O2 reduction in alkaline medium. Mater Lett 158:32–35
165. Ziwu L, Xin F, Meng L, Fang W, Quande W, Guojun K, Feng P (2015) Novel silicon-doped, silicon and nitrogen-codoped carbon nanomaterials with high activity for the oxygen reduction reaction in alkaline medium. J Mater Chem A 3:3289–3293
166. Syed CA, Kui D, Qin L, Yiyin H, Yakun B, Jing W, Jiangquan L, Muhammad AG, Yaobing W (2016) Si–C–F decorated porous carbon materials: a new class of electrocatalysts for the oxygen reduction reaction. J Mater Chem A 4:7924–7929
167. Mehdi DE, Parisa N (2017) Potential of Si-doped boron nitride nanotubes as a highly active and metal-free electrocatalyst for oxygen reduction reaction: a DFT study. Synth Met 226:129–138
168. In-Yup J, Min C, Hyun-Jung C, Sun-Min J, Min-Jung K, Jeong-Min S, Seo-Yoon B, Seonyoung Y, Guntae K, Hu YJ, Noejung P,

Jong-Beom B (2016) Antimony-doped graphene nanoplatelets. Nat Commun 6:7123–7131
169. Ziwu L, Meng L, Fang W, Quan-De W (2016) Novel as-doped, as and N-codoped carbon nanotubes as highly active and durable electrocatalysts for O_2 reduction in alkaline medium. J Power Sources 306:535–540
170. Qiliang W, Xiaohua Y, Gaixia Z, Dongniu W, Lucia Z, Dustin B, Lijun Y, Siyu Y, Youling W, Mohamed M, Shuhui S (2018) An active and robust Si-Fe/N/C catalyst derived from waste reed for oxygen reduction. Appl Catal B Environ 237:85–93
171. Sami U, Muhammad AUD, Muhammad UH, Shafqat A, Raheel A, Zhanpeng W, Dezhen W (2018) Oxygen reduction reaction of (C-PCTNB@CNTs): a nitrogen and phosphorus dual-doped carbon electro-catalyst derived from polyphosphazenes. J Power Sources 373:61–69
172. Kuldeep M, Deeksha J, Dmitry Z, Gokhan C, Jennifer L, Gordon R, Anne CC, Umit SO (2016) Probing the oxygen reduction reaction active sites over nitrogen-doped carbon nanostructures (CNx) in acidic media using phosphate anion. ACS Catal 6:7249–7259
173. You-Lin L, Cheng-Xiang S, Xue-Yan X, Ping-Chuan S, Tie-Hong C (2015) Nitrogen-doped hierarchically porous carbon spheres as efficient metal-free electrocatalysts for an oxygen reduction reaction. J Power Sources 283:389–396
174. Shuo D, Anli S, Zhaoling M, Jianghong W, Li T, Shuangyin W (2015) N-, P- and S-tridoped graphene as metal-free electrocatalyst for oxygen reduction reaction. J Electroanal Chem 753:21–27
175. Xiongwei W, Li Y, Peiyi W (2017) Water-soluble triphenylphosphine-derived microgel as the template towards in-situ nitrogen, phosphorus co-doped mesoporous graphene framework for supercapacitor and electrocatalytic oxygen reduction. Chem Eng J 328:417–427
176. Hao L, Wen-Jie J, Yun Z, Shuai N, Tang T, Lin-Bo H, Yu-Yun C, Zidong W, Jin-Song H (2018) Self-terminated activation for high-yield production of N,P-codoped nanoporous carbon as an efficient metal-free electrocatalyst for Zn-air battery. Carbon 128:97–105
177. Chenghang Y, Xiaowei J, Xianghui W, Yingjie H, Chongtai W, Qiang L, Shijun L (2018) Nitrogen, sulfur co-doped carbon derived from naphthalene-based covalent organic framework as an efficient catalyst for oxygen reduction. ACS Appl Energy Mater 1: 161–166
178. Jiang H, Zhu Y, Feng Q, Su Y, Yang X, Li C (2014) Nitrogen and phosphorus dual-doped hierarchical porous carbon foams as efficient metal-free electrocatalysts for oxygen reduction reactions. Chem Eur J 20:3106–3112
179. Gong X, Liu S, Ouyang C, Strasser P, Yang R (2015) Nitrogen- and phosphorus-doped biocarbon with enhanced electrocatalytic activity for oxygen reduction. ACS Catal 5:920–927
180. Zhang J, Qu L, Shi G, Liu J, Chen J, Dai L (2016) N, P-codoped carbon networks as efficient metal-free bifunctional catalysts for oxygen reduction and hydrogen evolution reactions. Angew Chem Int Ed 55:2230–2234
181. Wang Q, Li Y, Wang K, Zhou J, Zhu L, Hu J, Cao X (2017) Mass production of porous biocarbon self-doped by phosphorus and nitrogen for cost-effective zinc–air batteries. Electrochim Acta 257:250–258
182. Zhu L, Wu J, Zhang Q, Li X, Li Y, Cao X (2018) Chemical-free fabrication of N, P dual-doped honeycomb-like carbon as an efficient electrocatalyst for oxygen reduction. J Colloid Interface Sci 510:32–38
183. Zhang J, Zhao Z, Xia Z, Dai L (2015) A metal-free bifunctional electrocatalyst for oxygen reduction and oxygen evolution reactions. Nat Nanotechnol 10:444–452
184. Ding W, Li L, Xiong K, Wang Y, Li W, Nie Y, Qi X, Wei Z (2015) Shape fixing via salt recrystallization: a morphology-controlled approach to convert nanostructured polymer to carbon nanomaterial as a highly active catalyst for oxygen reduction reaction. J Am Chem Soc 137:5414–5420
185. Congling L, Zhengyan C, Aiguo K, Yangyang N, Fantao K, Yongkui S (2018) High-rate oxygen electroreduction over metal-free graphene foams embedding P–N coupled moieties in acidic media. J Mater Chem A 6:4145–4151
186. Yang J, Sun H, Liang H, Ji H, Song L, Gao C, Xu H (2016) A highly efficient metal-free oxygen reduction electrocatalyst assembled from carbon nanotubes and graphene. Adv Mater 28:4606–4613
187. Wang H, Ding J, Zhang J, Wang C, Yang W, Ren H, Kong A (2016) Fluorine and nitrogen co-doped ordered mesoporous carbon as a metal-free electrocatalyst for oxygen reduction reaction. RSC Adv 6:79928–79933
188. Parthiban V, Balasubramaniam B, Karthikeyan J, Murugan P, Sahu AK (2016) Fluorine-enriched mesoporous carbon as efficient oxygen reduction catalyst: understanding the defects in porous matrix and fuel cell applications. Nanoscale Adv 1:4926–4937
189. Wu Q, Liang J, Yi JD, Meng DL, Shi PC, Huang YB, Cao R (2019) Unraveling the relationship between the morphologies of metal–organic frameworks and the properties of their derived carbon materials. Dalton Trans 48:7211–7217
190. Liu S, Zhang H, Zhao Q, Zhang X, Liu R, Ge X, Wang G, Zhao H, Cai W (2016) Metal-organic framework derived nitrogen-doped porous carbon@ graphene sandwich-like structured composites as bifunctional electrocatalysts for oxygen reduction and evolution reactions. Carbon 106:74–83
191. Wu M, Li C, Zhao J, Ling Y, Liu R (2018) Tannic acid-mediated synthesis of dual-heteroatom-doped hollow carbon from a metal–organic framework for efficient oxygen reduction reaction. Dalton Trans 47:7812–7818
192. Tan ADD, Wang YF, Fu ZY, Tsiakaras P, Liang ZX (2017) Highly effective oxygen reduction reaction electrocatalysis: nitrogen-doped hierarchically mesoporous carbon derived from interpenetrated nonporous metal-organic frameworks. Appl Catal B Environ 218:260–266
193. Zhao R, Xia W, Lin C, Sun J, Mahmood A, Wang Q, Qiu B, Tabassum H, Zou RA (2017) Pore-expansion strategy to synthesize hierarchically porous carbon derived from metal-organic framework for enhanced oxygen reduction. Carbon 114:284–290
194. Zhong HX, Wang J, Zhang YW, Xu WL, Xing W, Xu D, Zhang YF, Zhang XB (2014) ZIF-8 derived graphene-based nitrogen-doped porous carbon sheets as highly efficient and durable oxygen reduction electrocatalysts. Angew Chem Int Ed 53:14235–14239
195. Zhang W, Wu ZY, Jiang HL, Yu SH (2014) Nanowire-directed templating synthesis of metal–organic framework nanofibers and their derived porous doped carbon nanofibers for enhanced electrocatalysis. J Am Chem Soc 136:14385–14388
196. Wei J, Hu Y, Liang Y, Kong B, Zhang J, Song J, Bao Q, Simon GP, Jiang S, Wang H (2015) Nitrogen-doped nanoporous carbon/graphene nano-sandwiches: synthesis and application for efficient oxygen reduction. Adv Funct Mater 25:5768–5777
197. Ge L, Yang Y, Wang L, Zhou W, Marco R, Chen Z, Zou J, Zhu Z (2015) High activity electrocatalysts from metal–organic framework-carbon nanotube templates for the oxygen reduction reaction. Carbon 82:417–424
198. Ma X, Zhao X, Sun J, Li D, Yang X (2016) A versatile strategy to fabricate MOFs/carbon material integrations and their derivatives for enhanced electrocatalysis. RSC Adv 6:7728–7735
199. Chung D, Lee K, Yu S, Kim M, Lee S, Kim O, Park H, Sung Y (2015) Alveoli-inspired facile transport structure of N-doped porous carbon for electrochemical energy applications. Adv Energy Mater 5:1401309–1401317
200. Shi PC, Yi JD, Liu TT, Li L, Zhang LJ, Sun CF, Wang YB, Huang YB, Cao R (2017) Hierarchically porous nitrogen-doped carbon nanotubes derived from core–shell ZnO@zeolitic imidazolate

framework nanorods for highly efficient oxygen reduction reactions. J Mater Chem A 5:12322–12329
201. Pandiaraj S, Aiyappa HB, Banerjee R, Kurungot S (2014) Post modification of MOF derived carbon via g-C3N4 entrapment for an efficient metal-free oxygen reduction reaction. Chem Commun 50:3363–3366
202. Li J, Chen Y, Tang Y, Li S, Dong H, Li K, Han M, Lan YQ, Bao J, Dai Z (2014) Metal–organic framework templated nitrogen and sulfur co-doped porous carbons as highly efficient metal-free electrocatalysts for oxygen reduction reactions. J Mater Chem A 2:6316–6319
203. Li J, Li S, Tang Y, Li K, Zhou L, Kong N, Lan Y, Bao J, Dai Z (2014) Heteroatoms ternary-doped porous carbons derived from MOFs as metal-free electrocatalysts for oxygen reduction reaction. Sci Rep 4:5130–5138
204. Zhang P, Sun F, Xiang Z, Shen Z, Yun J, Cao D (2014) ZIF-derived in situ nitrogen-doped porous carbons as efficient metal-free electrocatalysts for oxygen reduction reaction. Energy Environ Sci 7:442–450
205. Fu YA, Huang Y, Xiang ZH, Liu GQ, Cao DP (2016) Phosphorous–nitrogen-codoped carbon materials derived from metal–organic frameworks as efficient electrocatalysts for oxygen reduction reactions. Eur J Inorg Chem 2016:2100–2105
206. Li L, Dai P, Gu X, Wang Y, Yan L, Zhao X (2017) High oxygen reduction activity on a metal–organic framework derived carbon combined with high degree of graphitization and pyridinic-N dopants. J Mater Chem A 5:789–795
207. Higgins DC, Chen Z (2010) Nitrogen doped carbon nanotube thin films as efficient oxygen reduction catalyst for alkaline anion exchange membrane fuel cell. ECS Trans 28:63–68
208. Kruusenberg I, Ratso S, Vikkisk M, Kanninen P, Kallio T, Kannan AM, Tammeveski K (2015) Highly active nitrogen-doped nanocarbon electrocatalysts for alkaline direct methanol fuel cell. J Power Sources 281:94–102
209. Kumar MP, Raju MM, Arunchander A, Selvaraj S, Kalita G, Narayanan TN, Sahu AK, Pattanayak DK (2016) Nitrogen doped graphene as metal free electrocatalyst for efficient oxygen reduction reaction in alkaline media and its application in anion exchange membrane fuel cells. J Electrochem Soc 163:F848–F855
210. Chen J, Wang X, Cui X, Yang G, Zheng W (2014) Amorphous carbon enriched with pyridinic nitrogen as an efficient metal-free electrocatalyst for oxygen reduction reaction. Chem Commun 50:557–559
211. Palaniselvam T, Valappil MO, Illathvalappil R, Kurungot S (2014) Nanoporous graphene by quantum dots removal from graphene and its conversion to a potential oxygen reduction electrocatalyst via nitrogen doping. Energy Environ Sci 7:1059–1067
212. Unni SM, Bhange SN, Illathvalappil R, Mutneja N, Patil KR, Kurungot S (2015) Nitrogen-induced surface area and conductivity modulation of carbon nanohorn and its function as an efficient metal-free oxygen reduction electrocatalyst for anion-exchange membrane fuel cells. Small 11:352–360
213. To JWF, Ng JWD, Siahrostami S, Koh AL, Lee Y, Chen Z, Fong KD, Chen S, He J, Bae WG, Wilcox J, Jeong HY, Kim K, Studt F, Norskov JK, Jaramillo TF, Bao Z (2017) High-performance oxygen reduction and evolution carbon catalysis: from mechanistic studies to device integration. Nano Res 10:1163–1177
214. Lu Y, Wang L, Preuß K, Qiao M, Titirici MM, Varcoe J, Cai Q (2017) Halloysite-derived nitrogen doped carbon electrocatalysts for anion exchange membrane fuel cells. J Power Sources 372:82–90
215. Klingele M, Pham C, Vuyyuru KR, Britton B, Holdcroft S, Fischer A, Thiele S (2017) Sulfur doped reduced graphene oxide as metal-free catalyst for the oxygen reduction reaction in anion and proton exchange fuel cells. Electrochem Commun 77:71–75
216. Li J, Zhang Y, Zhang X, Huang J, Han J, Zhang Z, Han X, Xu P, Song B (2017) S, N dual-doped graphene-like carbon nanosheets as efficient oxygen reduction reaction electrocatalysts. ACS Appl Mater Interfaces 9:398–405
217. Lee S, Choun M, Ye Y, Lee J, Mun Y, Kang E, Hwang J, Lee YH, Shin CH, Moon SH, Kim SK, Lee E, Lee J (2015) Designing a highly active metal-free oxygen reduction catalyst in membrane electrode assemblies for alkaline fuel cells: effects of pore size and doping-site position. Angew Chem Int Ed 54:9230–3234
218. Xu N, Zhu T, Qiao J, Zhang F, Chen Z (2016) Nitrogen and sulfur co-doped mesoporous carbon as cathode catalyst for H2/O2 alkaline membrane fuel cell – effect of catalyst/bonding layer loading. Int J Hydrog Energy 41:9159–9166
219. Qiu Y, Huo J, Jia F, Shanks BH, Li W (2016) N- and S-doped mesoporous carbon as metal-free cathode catalysts for direct biorenewable alcohol fuel cells. J Mater Chem A 4:83–95
220. Kim OH, Cho YH, Chung DY, Kim MJ, Yoo JM, Park JE, Choe H, Sung YE (2015) Facile and gram-scale synthesis of metal-free catalysts: toward realistic applications for fuel cells. Sci Rep 5:8376–8384
221. Sa YJ, Park C, Jeong HY, Park SH, Lee Z, Kim KT, Park GG, Joo SH (2014) Carbon nanotubes/heteroatom-doped carbon core–sheath nanostructures as highly active, metal-free oxygen reduction electrocatalysts for alkaline fuel cells. Angew Chem Int Ed 53:4102–4106
222. Shui J, Wang M, Du F, Dai L (2015) N-doped carbon nanomaterials are durable catalysts for oxygen reduction reaction in acidic fuel cells. Sci Adv 1:e1400129–e1400136
223. Oh HS, Oh JG, Lee WH, Kim HJ, Kim H (2011) The influence of the structural properties of carbon on the oxygen reduction reaction of nitrogen modified carbon based catalysts. Int J Hydrog Energy 36:8181–8186
224. Subramanian NP, Li X, Nallathambi V, Kumaraguru SP, Colon-Mercado H, Wu G, Lee JW, Popov BN (2009) Nitrogen modified carbon-based catalysts for oxygen reduction reaction in polymer electrolyte membrane fuel cells. J Power Sources 188:38–44
225. Zhong H, Deng C, Qiu Y, Yao L, Zhang H (2014) Nitrogen doped hierarchically porous carbon as efficient oxygen reduction electrocatalysts in acid electrolyte. J Mater Chem A 2:17047–17057
226. Jin H, Zhang H, Zhong H, Zhang J (2011) Nitrogen-doped carbon xerogel: a novel carbon-based electrocatalyst for oxygen reduction reaction in proton exchange membrane (PEM) fuel cells. Energy Environ Sci 4:3389–3394